

SUPPLEMENTARY INFORMATION

UNVEILING THE SOLUTION STRUCTURE OF A DNA DUPLEX WITH CONTINUOUS SILVER-MODIFIED WATSON-CRICK BASE PAIRS

Uroš Javornik¹, Antonio Pérez-Romero², Carmen López-Chamorro², Rachelle M. Smith³, José A. Dobado⁴, Oscar Palacios⁵, Mrinal K. Bera⁶, May Nyman^{3,*}, Janez Plavec^{1,*}, and Miguel A. Galindo^{2,*}

¹ Slovenian NMR Center, National Institute of Chemistry and Faculty of Chemistry and Chemical Technology, University of Ljubljana, SI-1000 Ljubljana, Slovenia

² Departamento de Química Inorgánica, Universidad de Granada, 18001 Granada, Spain

³ Department of Chemistry, Oregon State University, Corvallis, OR 97331-4003, United States

⁴ Departamento de Química Orgánica, Universidad de Granada, 18001 Granada, Spain

⁵ Departament de Química, Universitat Autònoma de Barcelona, 08193 Cerdanyola del Vallès, Spain

⁶ NSF's ChemMatCARS, Pritzker School of Molecular Engineering, University of Chicago, Illinois 60637, United States

* To whom correspondence should be addressed: Miguel A. Galindo (magalindo@ugr.es); Janez Plavec (janez.plavec@ki.si); May Nyman (may.nyman@oregonstate.edu)

CONTENT

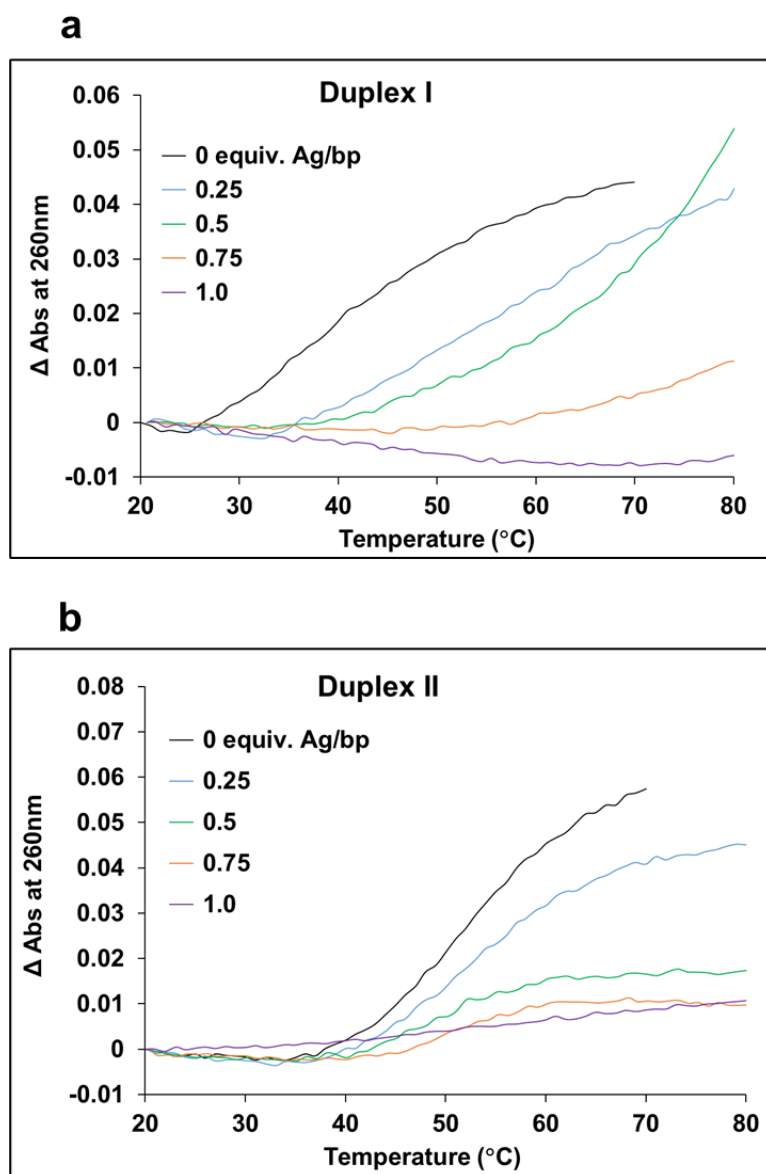
1. SUPPLEMENTARY METHODS	5
1.1 UV melting curves.	5
Supplementary Figure 1 UV-melting curves for duplex I and II in the presence of Ag ^I ions.	5
1.2 Circular Dichroism (CD) melting curves.	6
Supplementary Figure 2 CD-melting curves for duplex I and duplex II.	6
Supplementary Figure 3 CD-melting curves for duplex I and duplex II in the presence of Ag ^I ions	7
1.3 ESI-MS spectrometry for duplex I-Ag	8
Supplementary Figure 4 ESI-MS spectrum of duplex I in the presence of Ag ^I ions	8
Supplementary Table 1 Experimental and Theoretical masses for duplex I+Ag _n .	8
1.4 SAXS analysis.	8
Supplementary Figure 5 Scattering plots (from benchtop SAXS, Cu-K α radiation, 8.04 keV).	8
1.5 SAXS Fitting for Duplex I (0.7mM) (Anton Paar SAXSpace equipment).	9
Supplementary Figure 6. Pair distance distribution function analysis of duplex I	9
Supplementary Figure 7. Pair distance distribution function analysis of duplex I in the presence of 1 equivalent of Ag ^I per base pair	9
1.6 SAXS fitting figures for duplex I (0.2 mM) (K-edge; 25.514 keV) (Advanced Photon Source)	10
Supplementary Figure 8 Cylindrical model of duplex I (0.2 mM) in absence of Ag ^I (K-edge; 25.514 keV).	10
Supplementary Figure 9 Cylindrical model of duplex I (0.2 mM) upon adding 1 equivalent of Ag ^I per base pair (K-edge; 25.514 keV).	11
Supplementary Figure 10 Cylindrical model of duplex I (0.2 mM) upon adding 1.5 equivalents of Ag ^I per base pair (K-edge; 25.514 keV).	12
Supplementary Figure 11 Cylindrical model of duplex I (0.2 mM) upon adding 2 equivalents of Ag ^I per base pair (K-edge; 25.514 keV).	13
1.7 SAXS fitting figures for duplex I (0.2 mM) (K-edge; 24.514 keV) (Advanced Photon Source)	14
Supplementary Figure 12 Cylindrical model of duplex I (0.2 mM) in absence of Ag ^I ions (away from K-edge; 24.514 keV).	14
Supplementary Figure 13 Cylindrical model of duplex I (0.2 mM) upon adding 1 equivalent of Ag ^I per base pair (away from K-edge; 24.514 keV).	15
Supplementary Figure 14 Cylindrical model of duplex I (0.2 mM) upon adding 1.5 equivalents of Ag ^I per base pair (away from K-edge; 24.514 keV).	16
Supplementary Figure 15 Cylindrical model of duplex I (0.2 mM) upon adding 2 equivalents of Ag ^I per base pair (away from K-edge; 24.514 keV).	17
1.8 SAXS fitting figures for duplex II (0.2mM) (K-edge; 25.514 keV) (Advanced Photon Source)	18

Supplementary Figure 16 Cylindrical model of canonical duplex II (0.2 mM) in absence of Ag ^I (K-edge; 25.514 keV).....	18
Supplementary Figure 17 Cylindrical model of canonical duplex II (0.2 mM) upon adding 1 equivalent of Ag ^I per base pair (K-edge; 25.514 keV).....	19
Supplementary Figure 18 Cylindrical model of canonical duplex II (0.2 mM) upon adding 1.5 equivalents of Ag ^I per base pair (K-edge; 25.514 keV).	20
Supplementary Figure 19 Cylindrical model of canonical duplex II (0.2 mM) upon adding 2.0 equivalents of Ag ^I per base pair (K-edge; 25.514 keV).	21
1.9 SAXS fitting figures for duplex II (0.2 mM) (K-edge; 24.514 keV) (Advanced Photon Source)	22
Supplementary Figure 20 Cylindrical model of canonical duplex II (0.2 mM) in absence of Ag ^I (away from K-edge; 24.514 keV).....	22
Supplementary Figure 21 Cylindrical model of canonical duplex II (0.2 mM) upon adding 1 equivalent of Ag ^I per base pair (away from K-edge; 24.514 keV).....	23
Supplementary Figure 22 Cylindrical model of canonical duplex II (0.2 mM) upon adding 1.5 equivalents of Ag ^I per base pair (away from K-edge; 24.514 keV).	24
Supplementary Figure 23 Cylindrical model of canonical duplex II (0.2 mM) upon adding 2 equivalents of Ag ^I per base pair (away from K-edge; 24.514 keV).	25
Supplementary Table 2 Cylindrical fitting parameters for anomalous X-ray scattering of duplex I in the presence of Ag ^I ions.	26
Supplementary Table 3 Duplex I core-shell cylinder fit comparing Ag-core density at the silver K-edge (25.514 keV) and below the silver K-edge (24.514 keV).....	26
Supplementary Table 4 Duplex II core-shell cylinder fit comparing Ag-core density at the silver K-edge (25.514 keV) and below the silver K-edge (24.514 keV).....	27
Supplementary Figure 24 Comparison of scattering of duplex I in the presence and absence of Ag ^I at two different scattering energies.....	28
1.10 ASAXS Analysis	29
Supplementary Figure 25 The scattering components - SAXS-term (<i>IS</i>), Cross-term (<i>IC</i>), and Resonant-term (<i>IR</i>) obtained from energy dependent SAXS data below the X-ray absorption K-edge of Ag from duplex I with different Ag ^I equivalents.	31
Supplementary Figure 26 The scattering components - SAXS-term (<i>IS</i>), Cross-term (<i>IC</i>), and Resonant-term (<i>IR</i>) obtained from energy dependent SAXS data below the X-ray absorption K-edge of Ag from duplex II with different Ag ^I equivalents.	32
Supplementary Figure 27 Solid cylinder structure to model the Ag-DNA complexes in water.	33
1.11 NMR spectroscopy	35
Supplementary Figure 28 ¹ H NMR spectra of titration of the canonical analogue duplex II (5'-d(GGA CTC GAG TCC)-3' with Ag ^I ions.....	35
Supplementary Figure 29 ³¹ P NMR spectra of the duplex I before and after adding 2 equivalents of Ag ^I ions per base pair with assignments.	36
1.12 Comparison of average structural parameters for I and I-Ag structures	36

Supplementary Table 5. Comparison of average structural parameters for I , I-Ag (NMR) and I-Ag (DFT) structures along with typical B-DNA values.	36
Supplementary Table 6. Neighbouring Ag ^I ion distances in I-Ag (NMR) and I-Ag (DFT) structures.	37
1.13 RP-HPLC oligonucleotide analysis for ODN1.....	37
Supplementary Figure 30. RP-HPLC chromatogram (C18 column) of purified oligonucleotide ODN1.....	37
1.14 Mass Spectrometry for oligonucleotide ODN1 and ODN2	38
Supplementary Figure 31. ESI-MS (negative mode) spectra for oligonucleotide ODN1.	38
Supplementary Figure 32. ESI-MS (negative mode) spectra for canonical oligonucleotide ODN2.	39
2. SUPPLEMENTARY REFERENCES	40

1. SUPPLEMENTARY METHODS

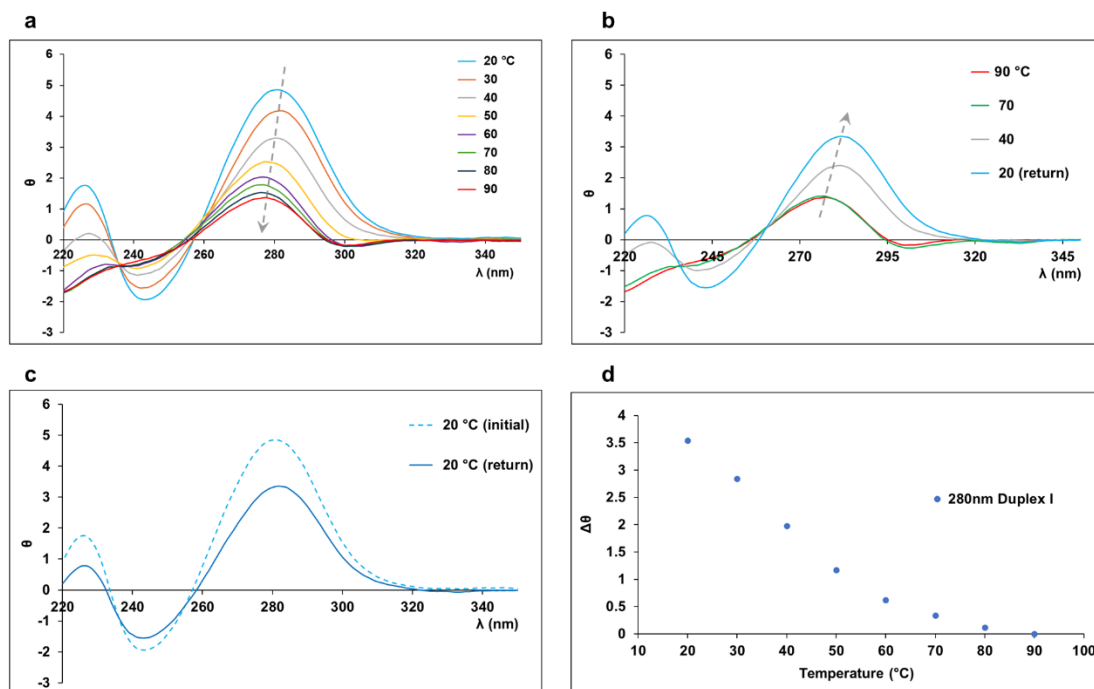
1.1 UV melting curves.



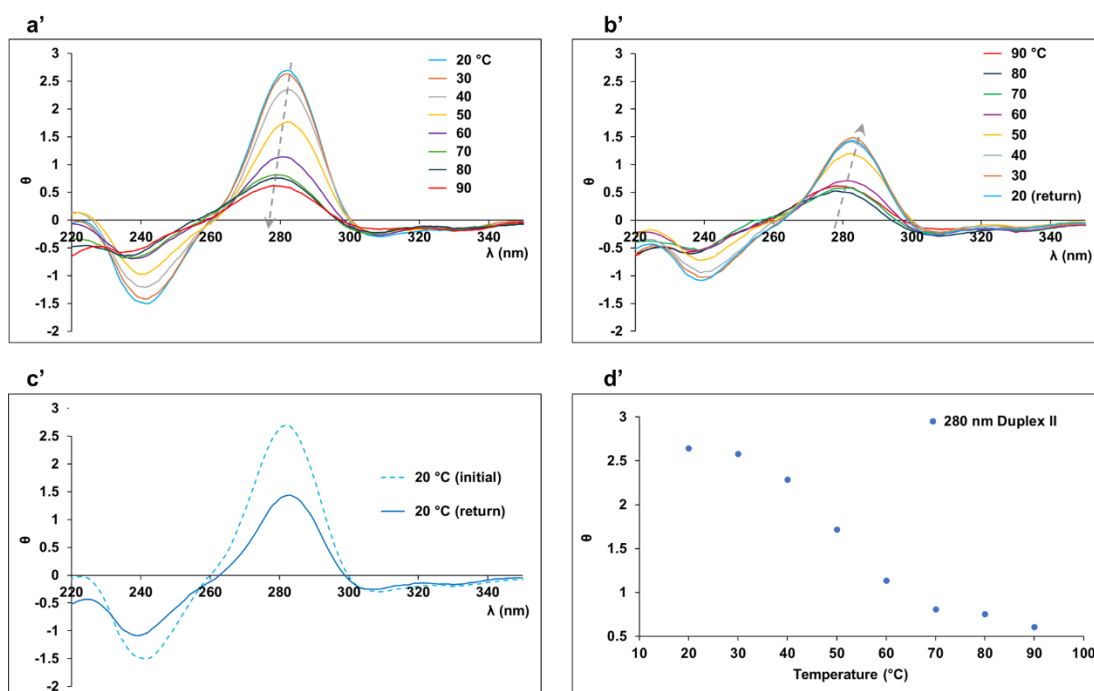
Supplementary Figure 1 | UV-melting curves for duplex I and II in the presence of Ag^+ ions registered at 260 nm. Relative values for melting curves for **a)** duplex I, and **b)** duplex II. Conditions: 2 μM duplex, 5 mM MOPS pH 8.5, 100 mM NaClO_4 , Ag^+ equivalents (equiv.) per base pair (bp) indicated in the inset.

1.2 Circular Dichroism (CD) melting curves.

Duplex I

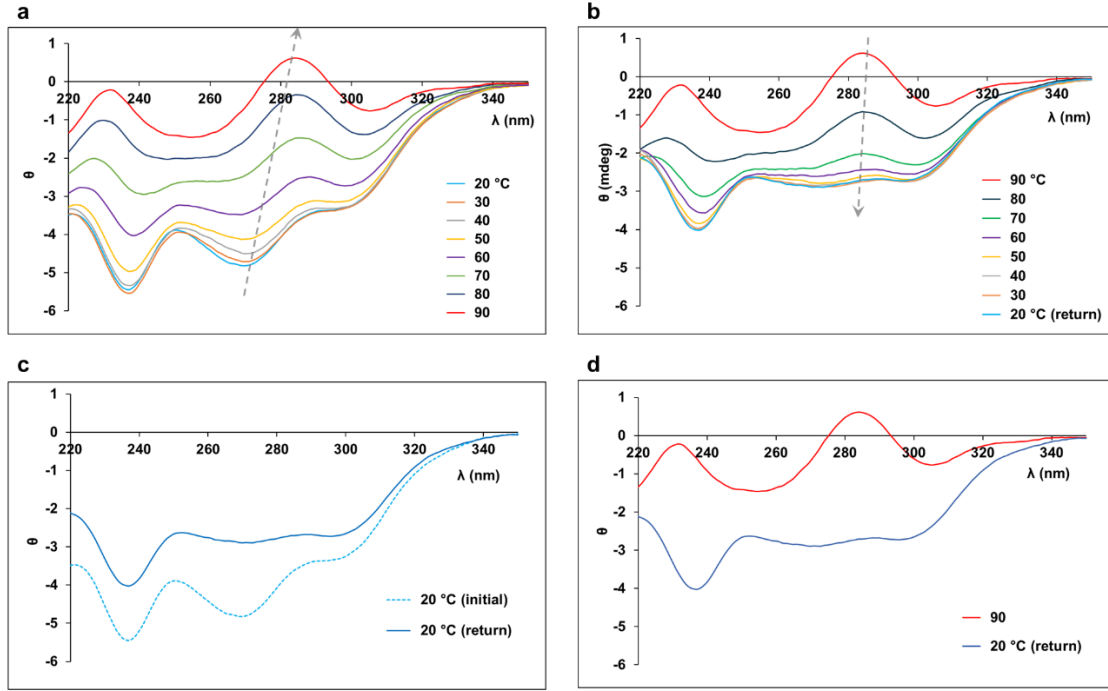


Duplex II (canonical)

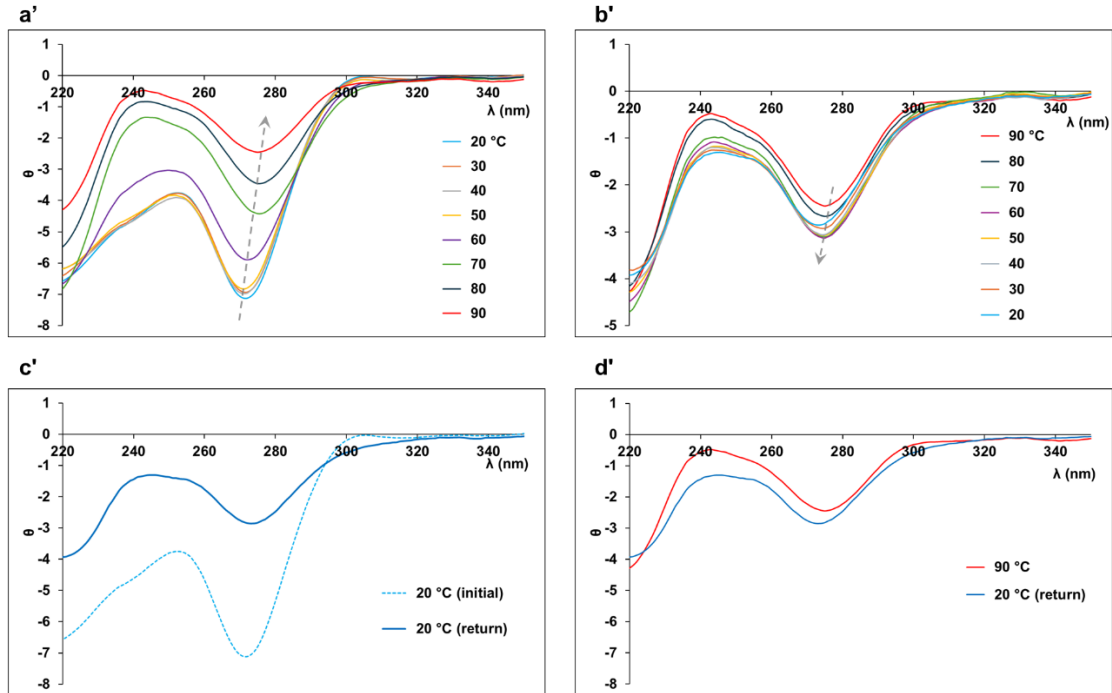


Supplementary Figure 2 | CD-melting curves for duplex I and duplex II. a,a') CD curves upon heating the sample, **b,b')** CD curves upon cooling the sample, **c,c')** Comparison of CD curves for sample at 20 °C before and after (return) the heating-cooling process, **d,d')** Ellipticities variation at 280 nm upon heating sample. Conditions: 2 μ M duplex, 5mM MOPS pH 8.5, 100 mM NaClO₄.

Duplex I -Ag

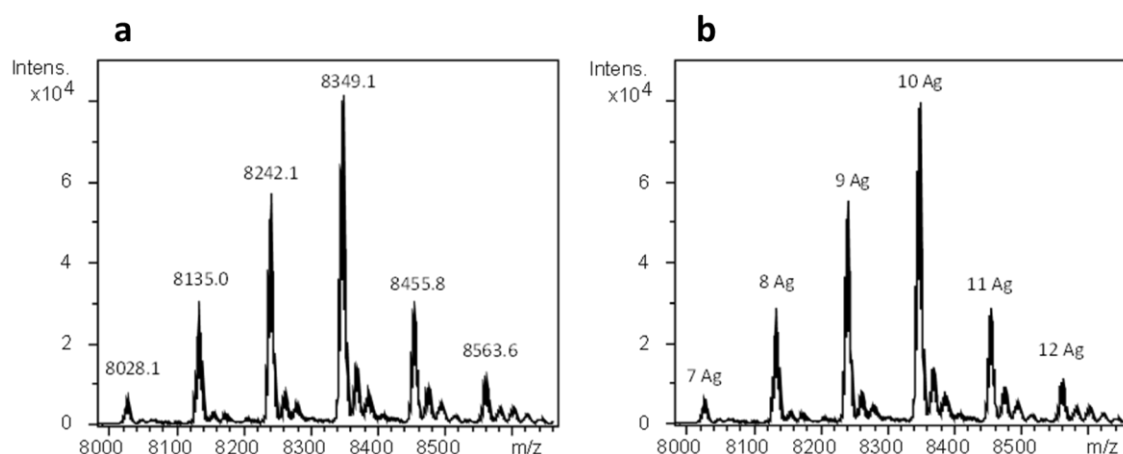


Duplex II-Ag



Supplementary Figure 3 | CD-melting curves for duplex I and duplex II in the presence of 1.1 equivalent of Ag^{I} ions per base pair (bp). a,a') CD curves upon heating the sample, **b,b')** CD curves upon cooling the sample, **c,c')** Comparison of CD spectrum at 20 °C before and after the heating-cooling process, **d,d')** Comparison of CD spectrum at 90 °C and 20 °C, after cooling process (return). Conditions: 2 μM duplex, 24 μM Ag^{I} , 5mM MOPS pH 8.5, 100 mM NaClO_4 .

1.3 ESI-MS spectrometry for Duplex I-Ag

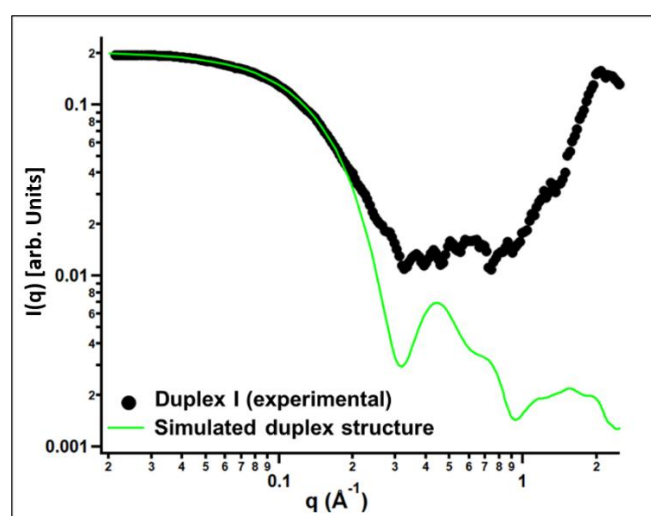


Supplementary Figure 4 | ESI-MS spectrum of duplex I in the presence of Ag^+ . **a**, Deconvoluted spectrum with the masses of different **I+Ag** complexes. **b**, Deconvoluted spectrum showing the corresponding equivalents of Ag^+ bound per duplex I. Conditions: 200 μM ds-DNA, 100 mM NaClO_4 , 100 mM Tris/ HNO_3 and 4.8 mM AgNO_3 water solution at pH 8.4.

Supplementary Table 1 | Experimental and Theoretical masses corresponding to the duplex I+ Ag_n

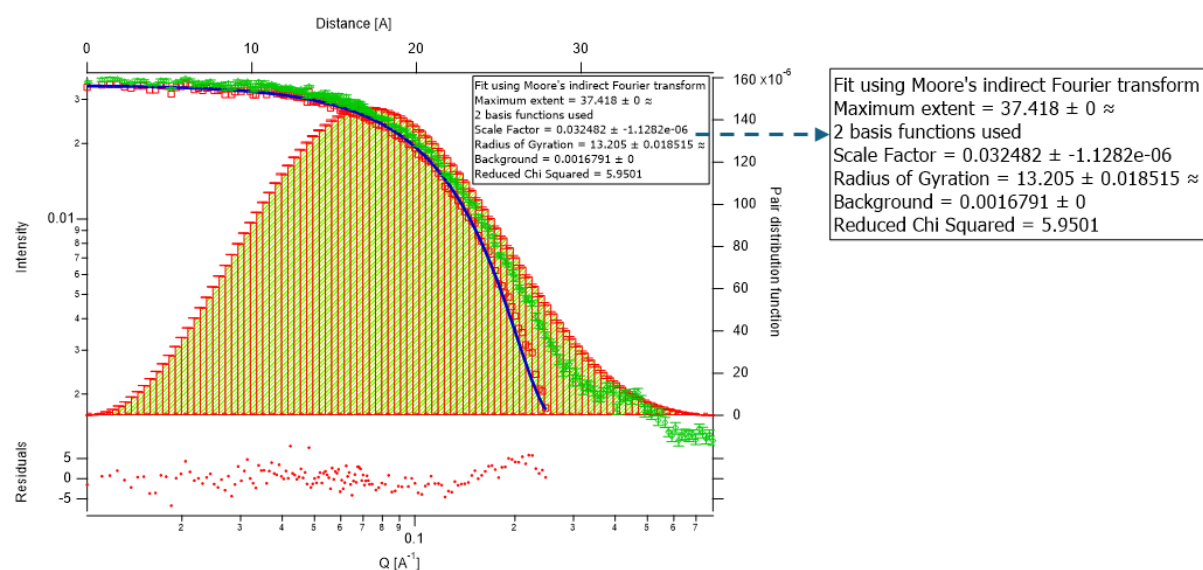
n	7	8	9	10	11	12
Found Mass	8028.1	8135.0	8242.1	8349.1	8455.8	8563.6
Calcd Mass	8027.93	8134.79	8241.64	8348.51	8455.37	8562.23

1.4 SAXS analysis

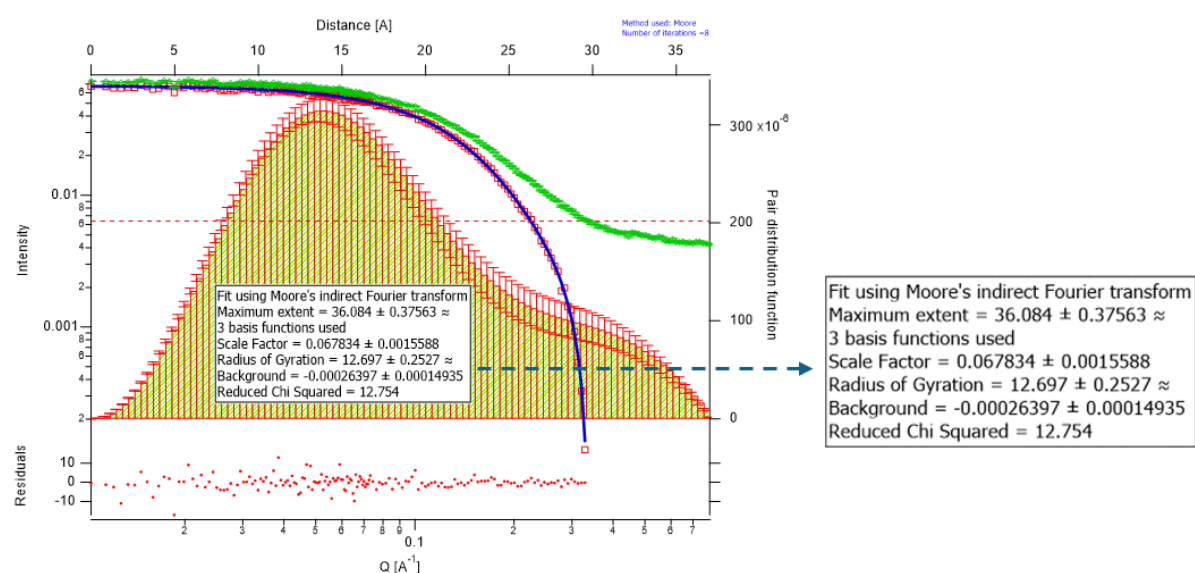


Supplementary Figure 5 | Scattering plots (from benchtop SAXS, Cu- $\text{K}\alpha$ radiation, 8.04 keV). Comparing experimental data obtained for duplex I and simulated scattering data for a 12-mer duplex form.

1.5 SAXS Fitting for Duplex I (0.7mM) (Anton Paar SAXSpace equipment).

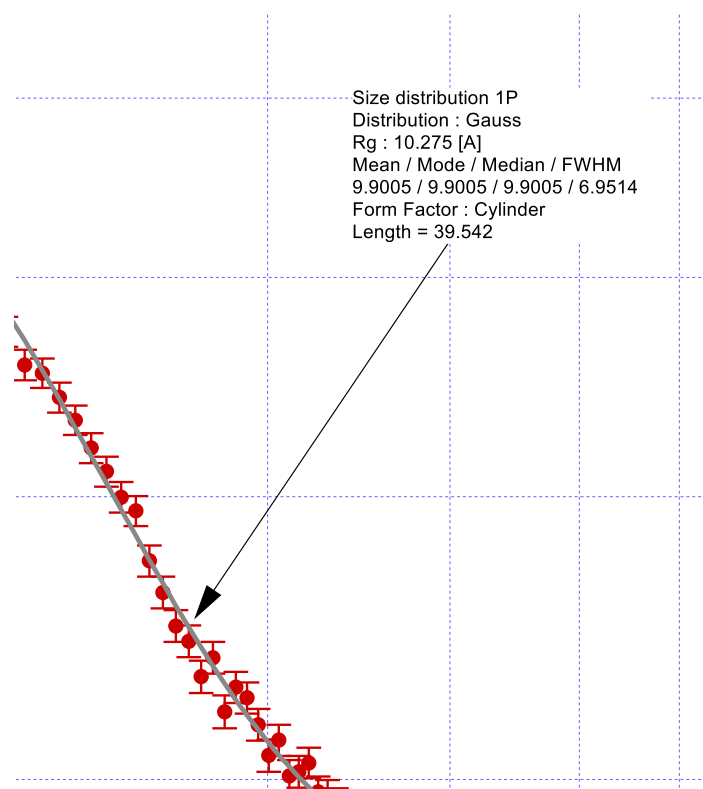
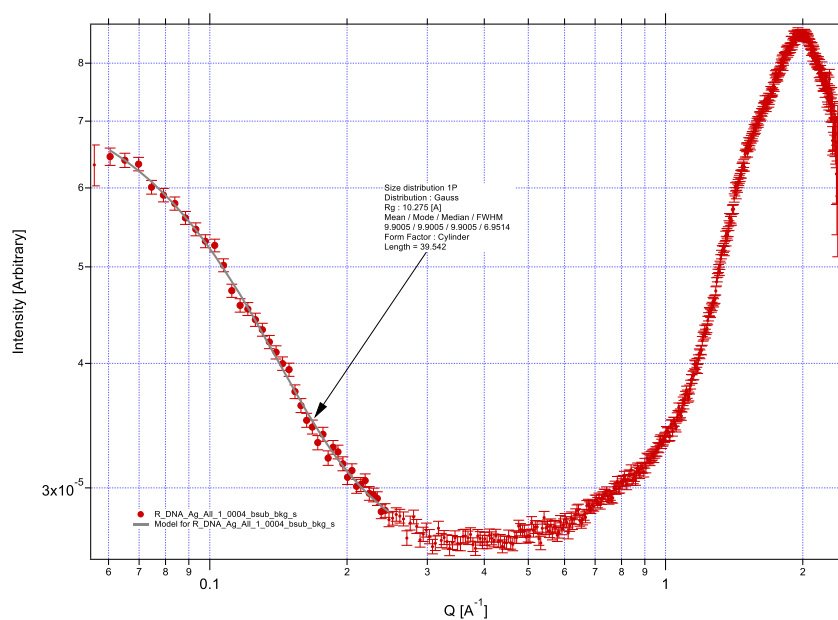


Supplementary Figure 6. Pair distance distribution function analysis of duplex I. The green data points are the original data, the red squares is the data minus a flat background for fitting, the blue line is the model fit. Parameters for fitting and obtained results summarized in the legend.

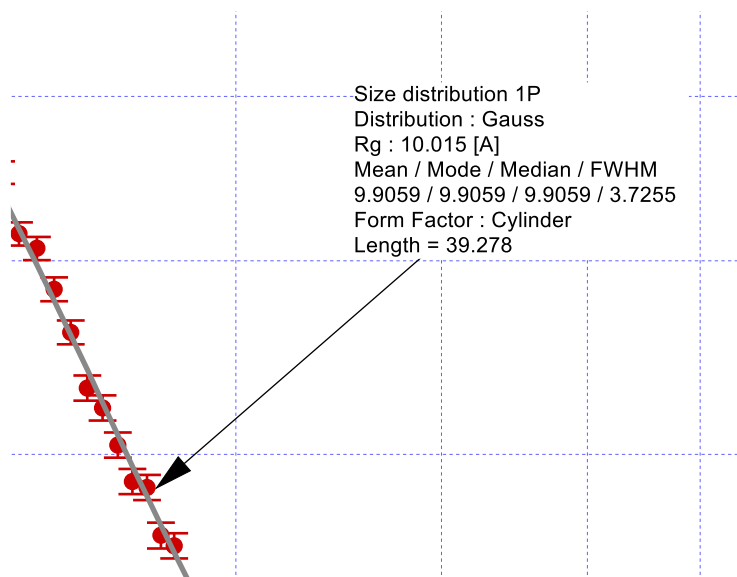
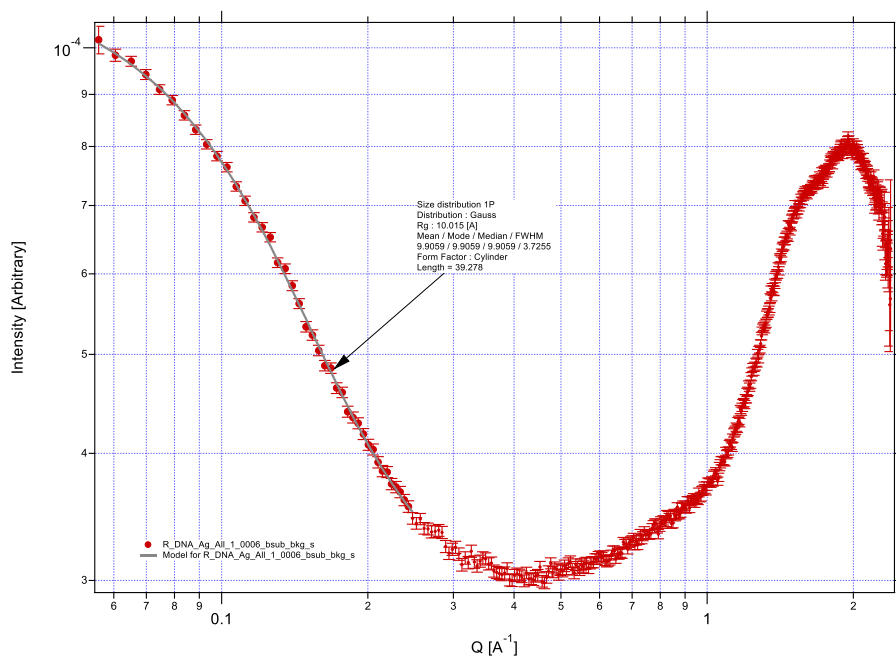


Supplementary Figure 7. Pair distance distribution function analysis of duplex I in the presence of 1 equivalent of Ag^+ per base pair. The green data points are the original data, the red squares is the data minus a flat background for fitting, the blue line is the model fit. Parameters for fitting and obtained results summarized in the legend.

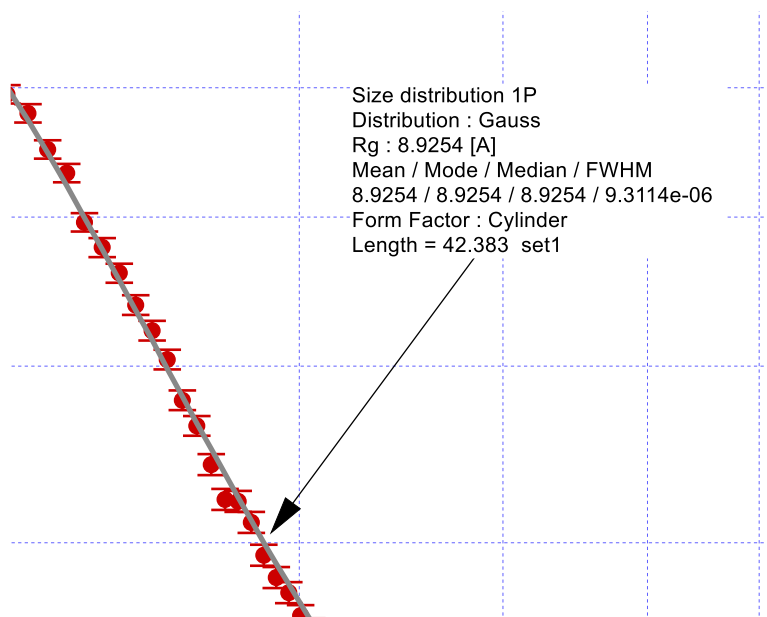
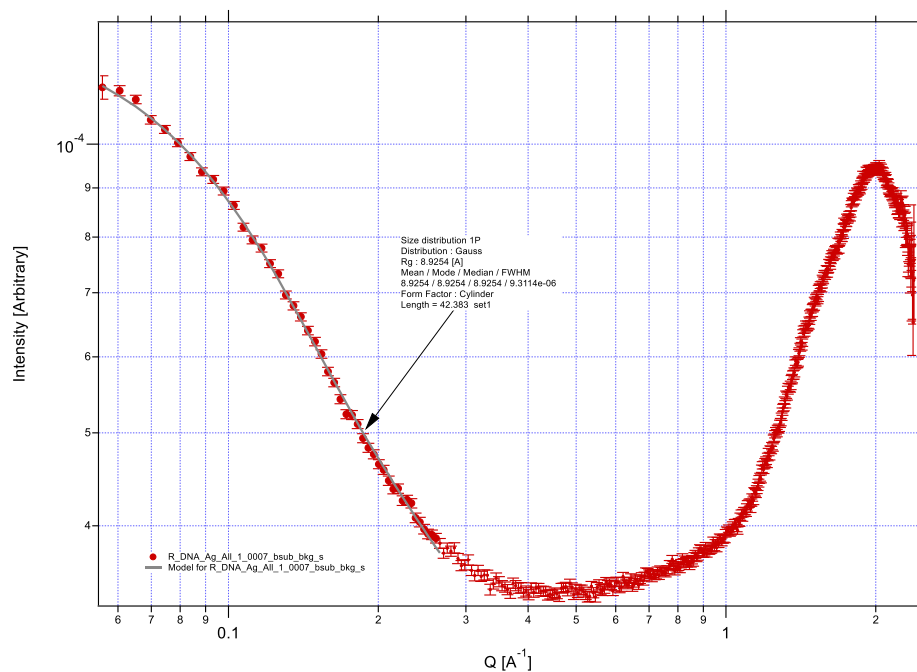
1.6 SAXS fitting figures for duplex I (0.2 mM) (K-edge; 25.514 keV) (Advanced Photon Source)



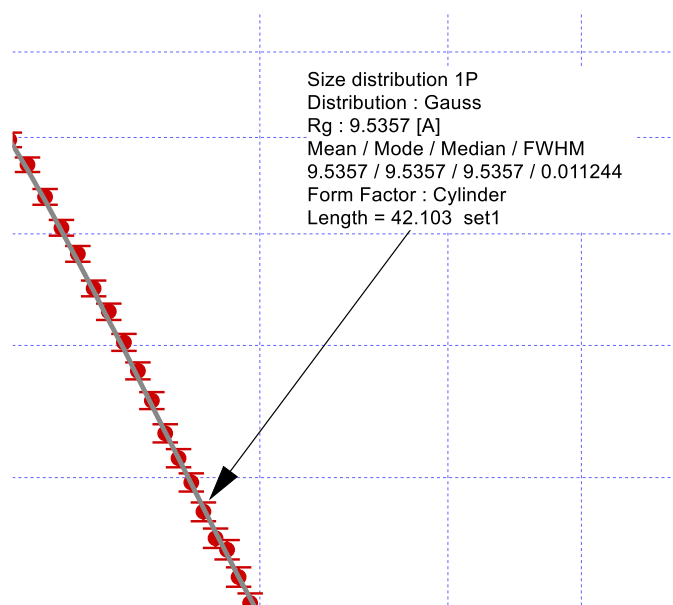
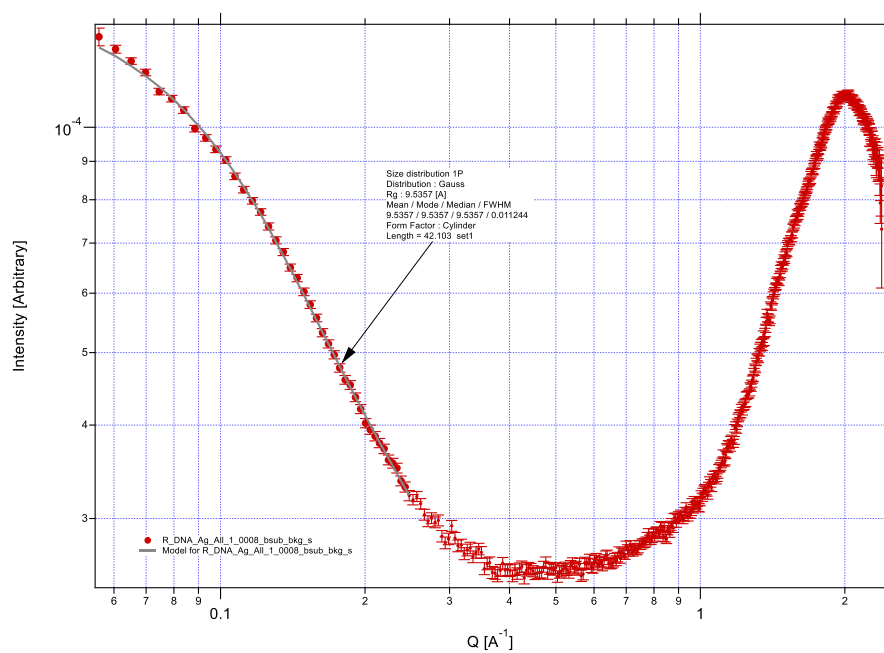
Supplementary Figure 8 | Cylindrical model of duplex I (0.2 mM) in absence of Ag^I ions (K-edge; 25.514 keV).



Supplementary Figure 9 | Cylindrical model of duplex I (0.2 mM) upon adding 1 equivalent of Ag^I per base pair (K-edge; 25.514 keV).

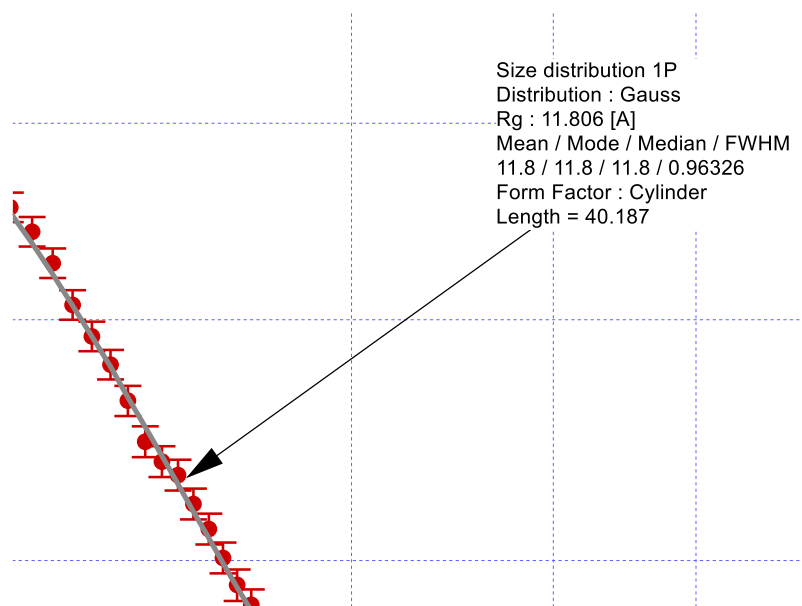
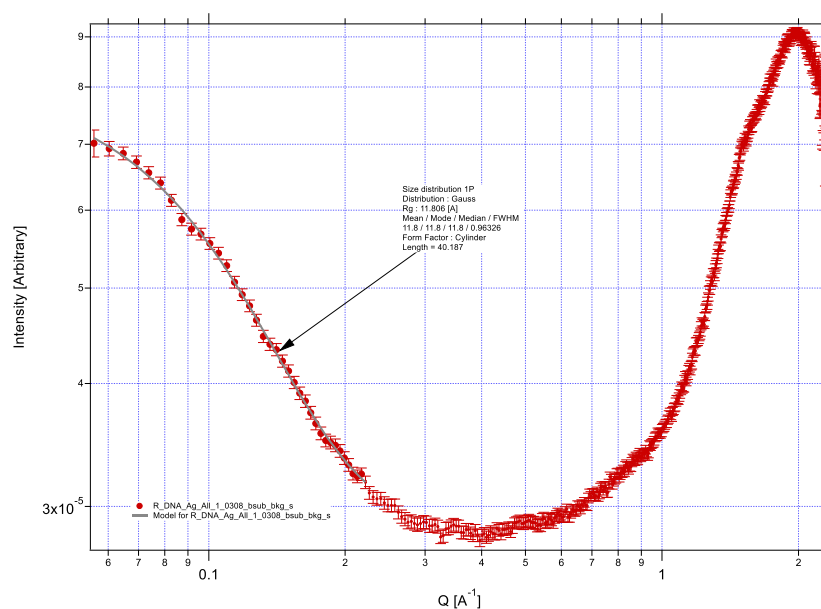


Supplementary Figure 10 | Cylindrical model of duplex I (0.2 mM) upon adding 1.5 equivalents of Ag^I per base pair (K-edge; 25.514 keV).

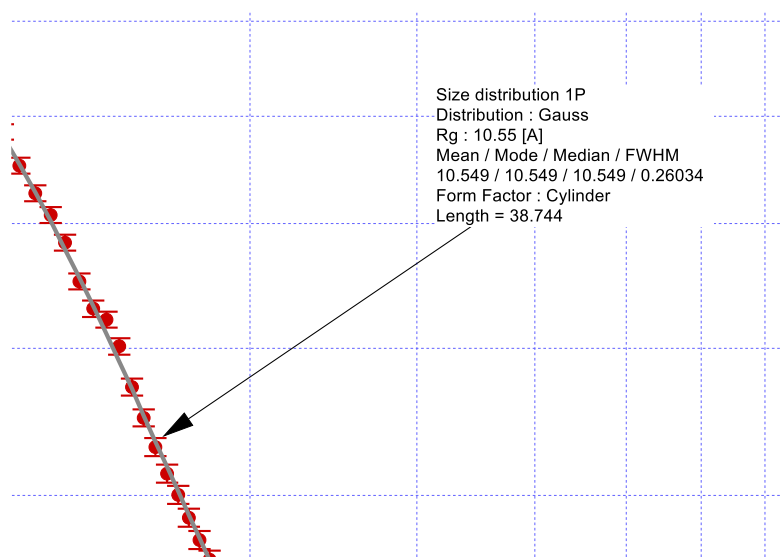
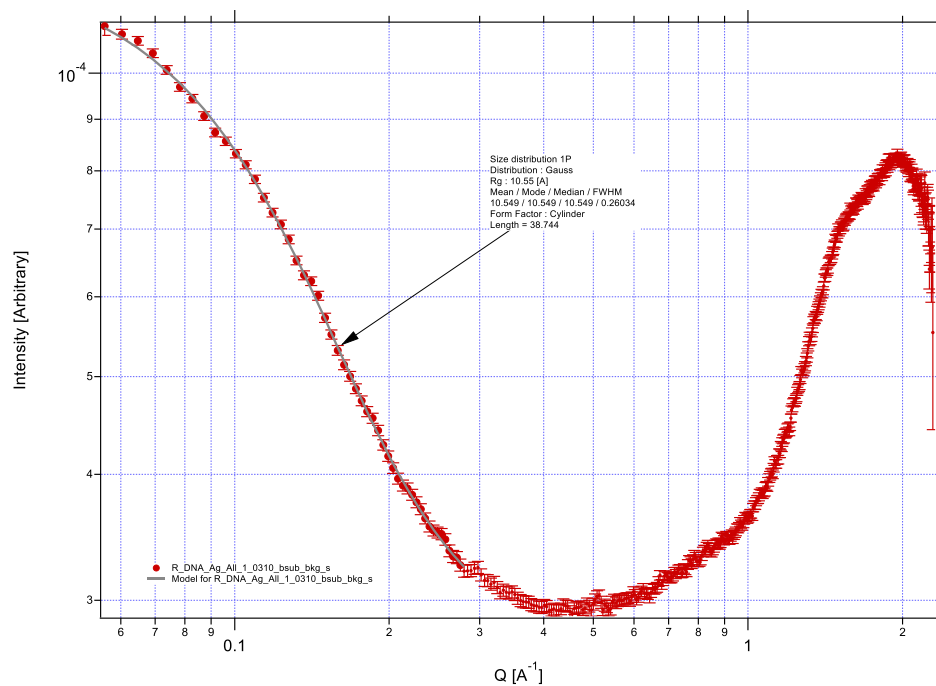


Supplementary Figure 11 | Cylindrical model of duplex I (0.2 mM) upon adding 2 equivalents of Ag^I per base pair (K-edge; 25.514 keV).

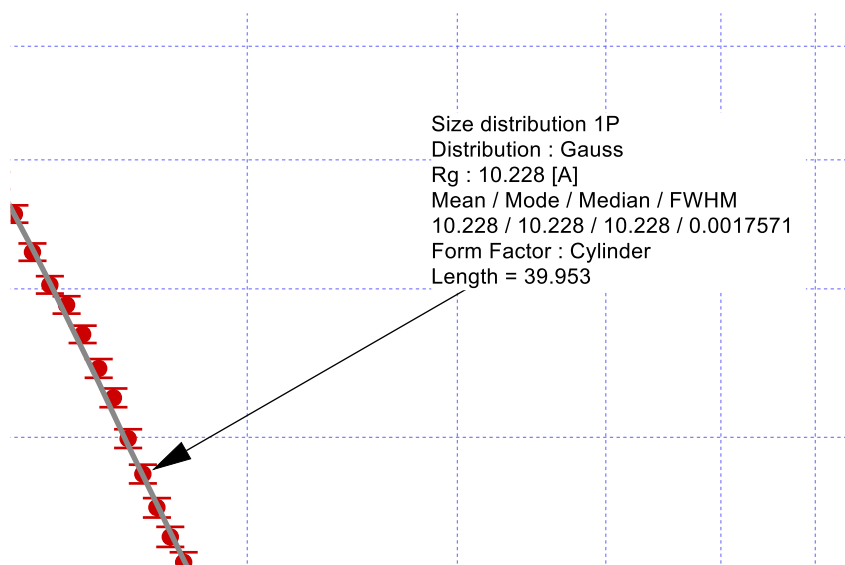
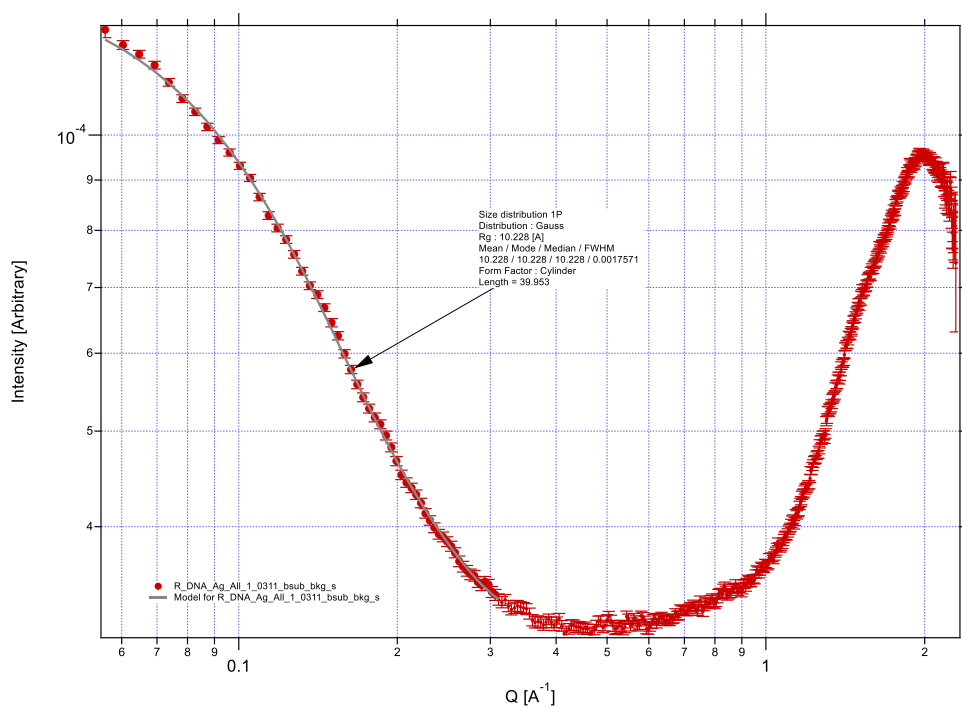
1.7 SAXS fitting figures for Duplex I (0.2 mM) (away K-edge; 24.514 keV)
(Advanced Photon Source)



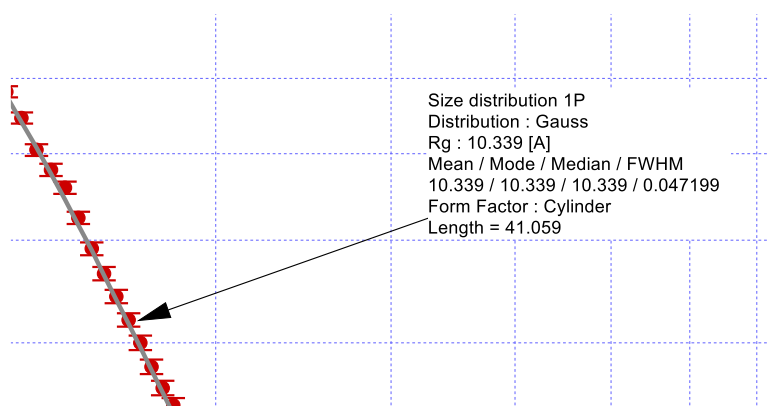
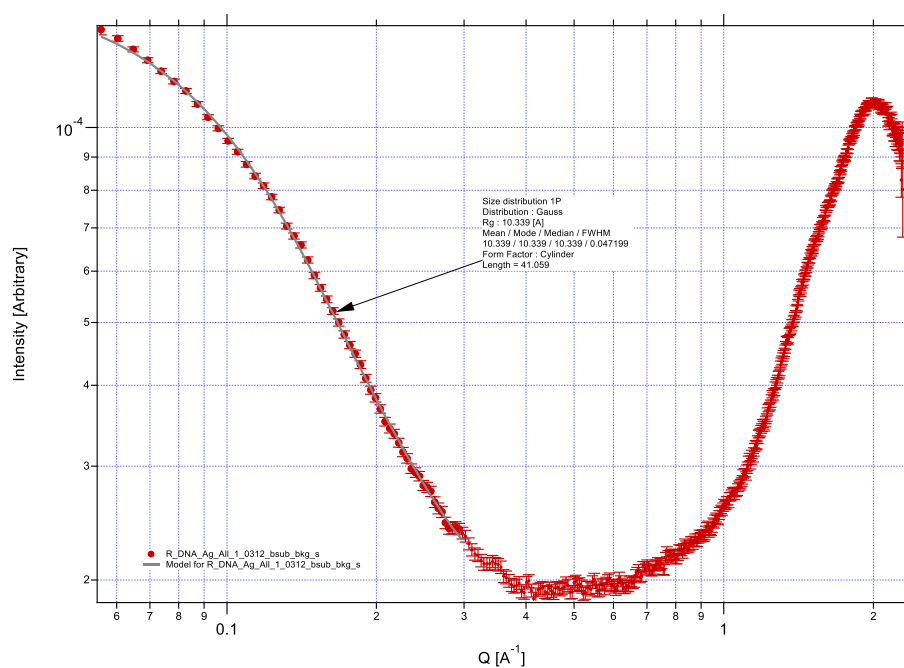
Supplementary Figure 12 | Cylindrical model of duplex I (0.2 mM) in absence of Ag^I ions (away from K-edge; 24.514 keV).



Supplementary Figure 13 | Cylindrical model of duplex I (0.2 mM) upon adding 1 equivalent of Ag^I per base pair (away from K-edge; 24.514 keV).

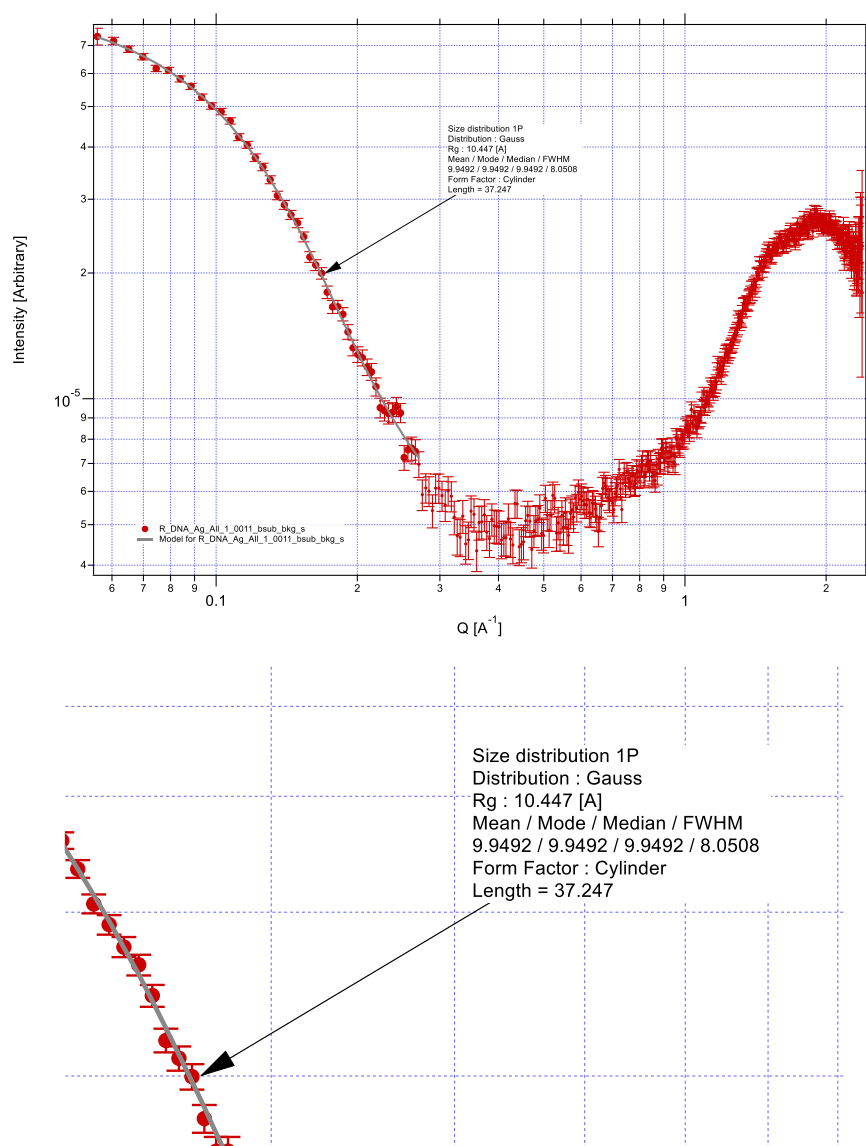


Supplementary Figure 14 | Cylindrical model of duplex I (0.2 mM) upon adding 1.5 equivalents of Ag^I per base pair (away from K-edge; 24.514 keV).

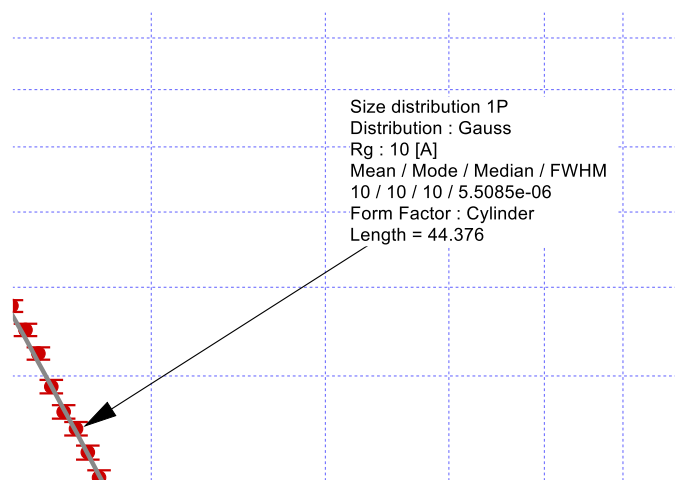
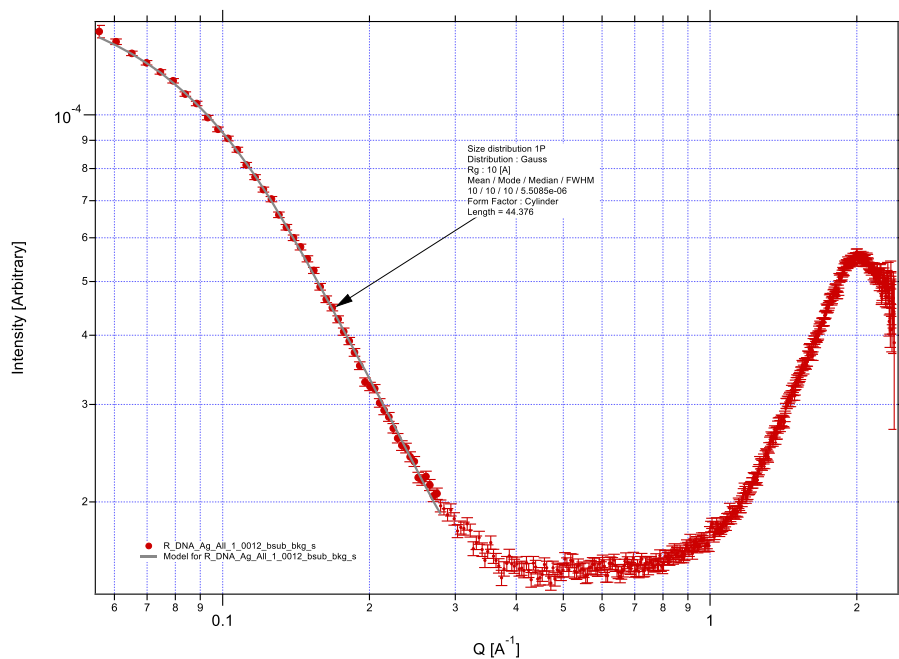


Supplementary Figure 15 | Cylindrical model of duplex I (0.2 mM) upon adding 2 equivalents of AgI per base pair (away from K-edge; 24.514 keV).

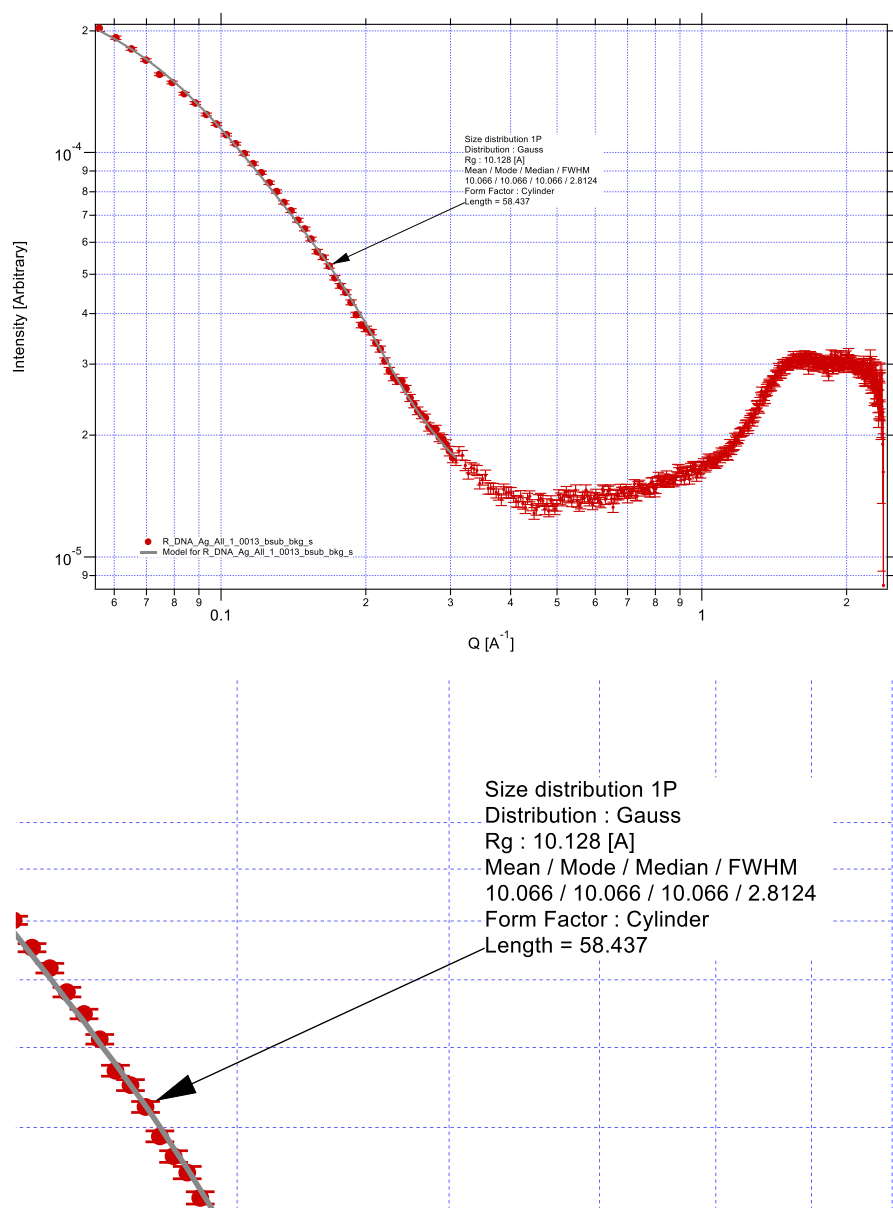
1.8 SAXS fitting figures for Duplex II (0.2mM) (K-edge; 25.514 keV) (Advanced Photon Source)



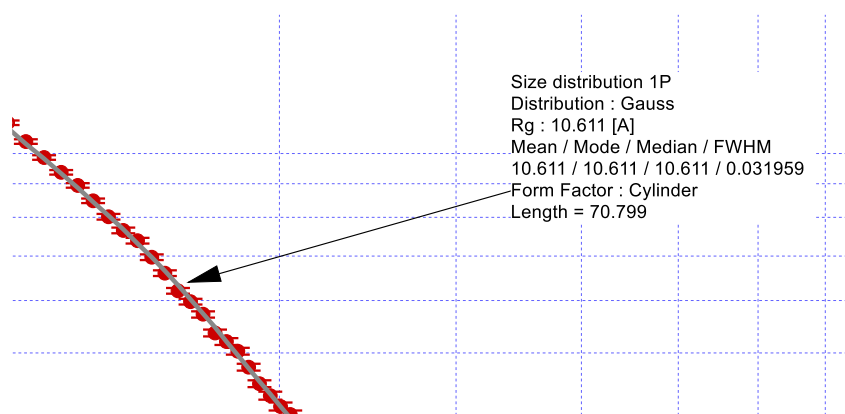
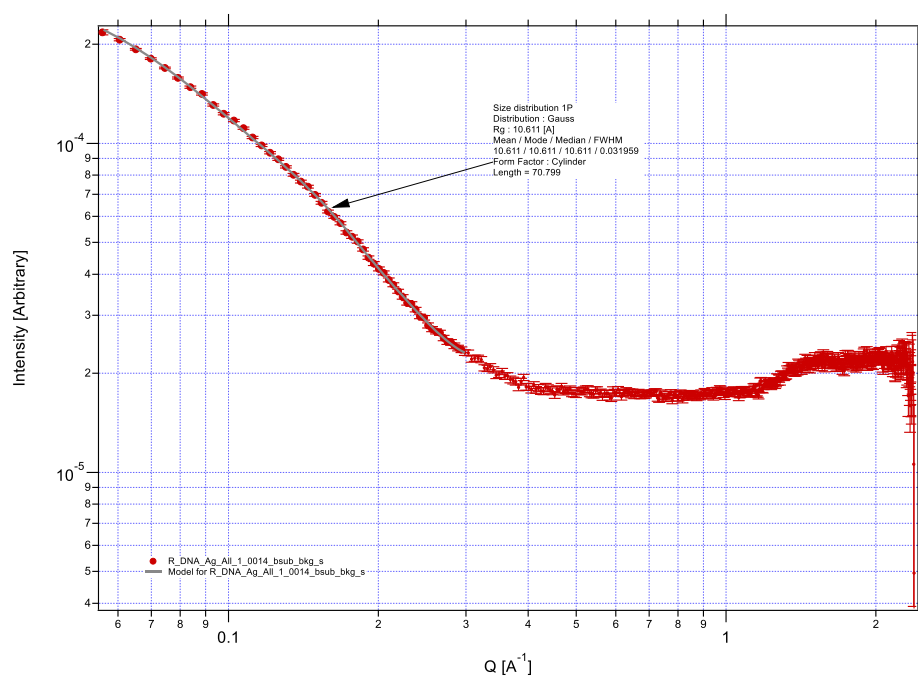
Supplementary Figure 16 | Cylindrical model of canonical duplex II (0.2 mM) in absence of Ag^I (K-edge; 25.514 keV).



Supplementary Figure 17 | Cylindrical model of canonical duplex II (0.2 mM) upon adding 1 equivalent of Ag^I per base pair (K-edge; 25.514 keV).

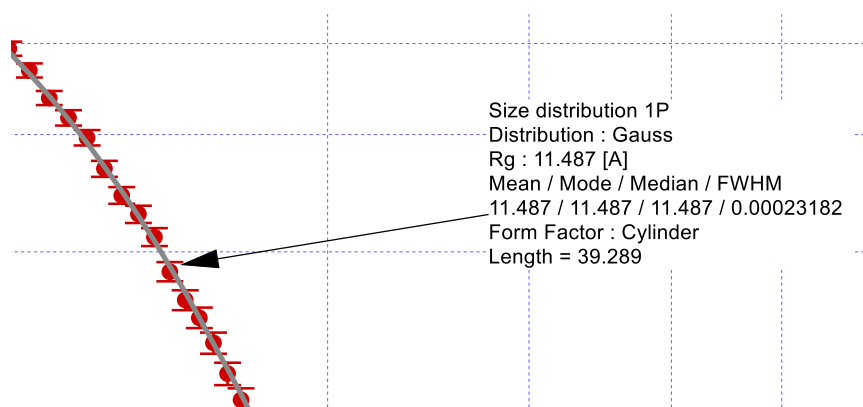
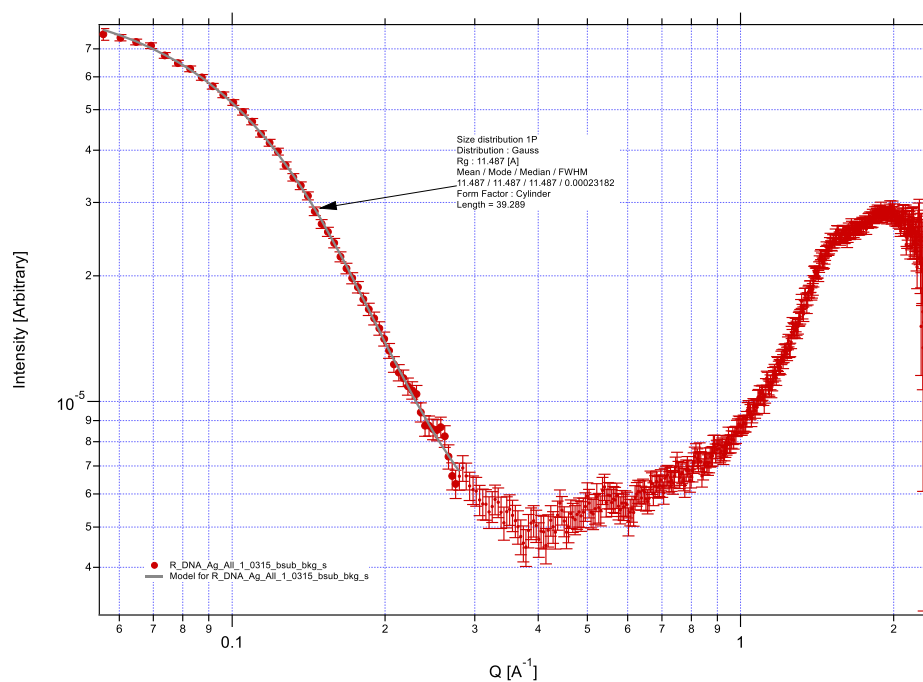


Supplementary Figure 18 | Cylindrical model of canonical duplex II (0.2 mM) upon adding 1.5 equivalents of Ag^I per base pair (K-edge; 25.514 keV).

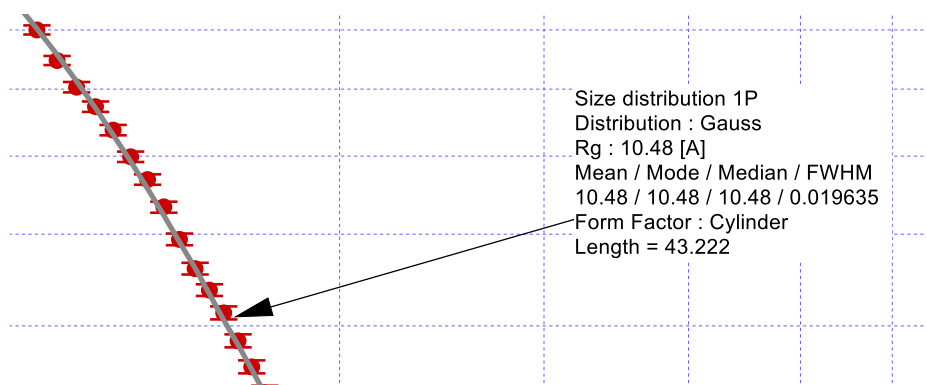
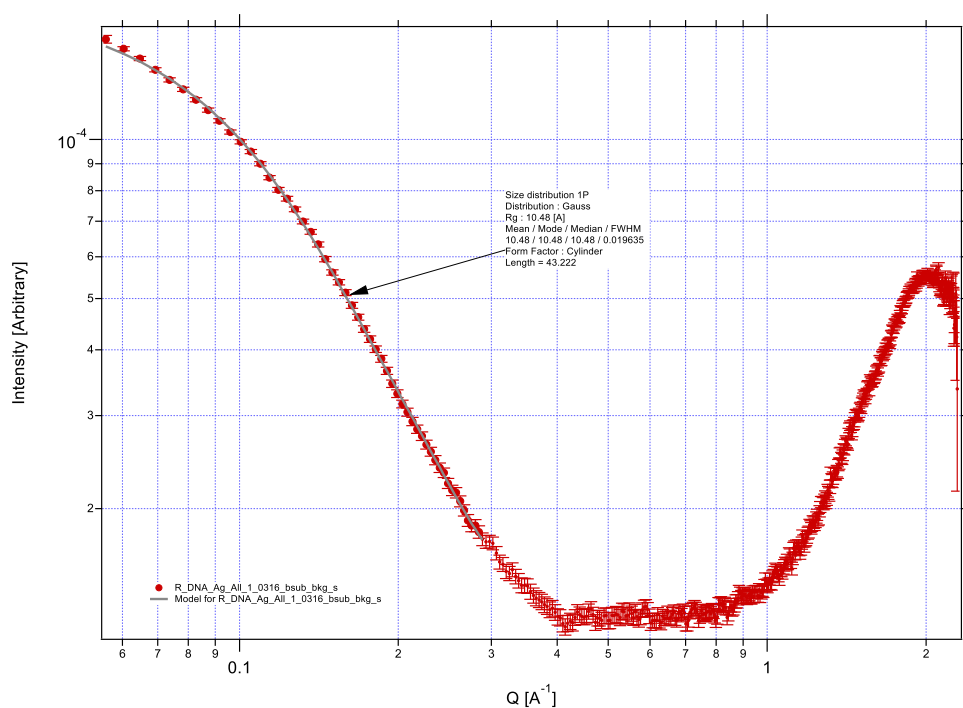


Supplementary Figure 19 | Cylindrical model of canonical duplex II (0.2 mM) upon adding 2.0 equivalents of Ag^I per base pair (K-edge; 25.514 keV).

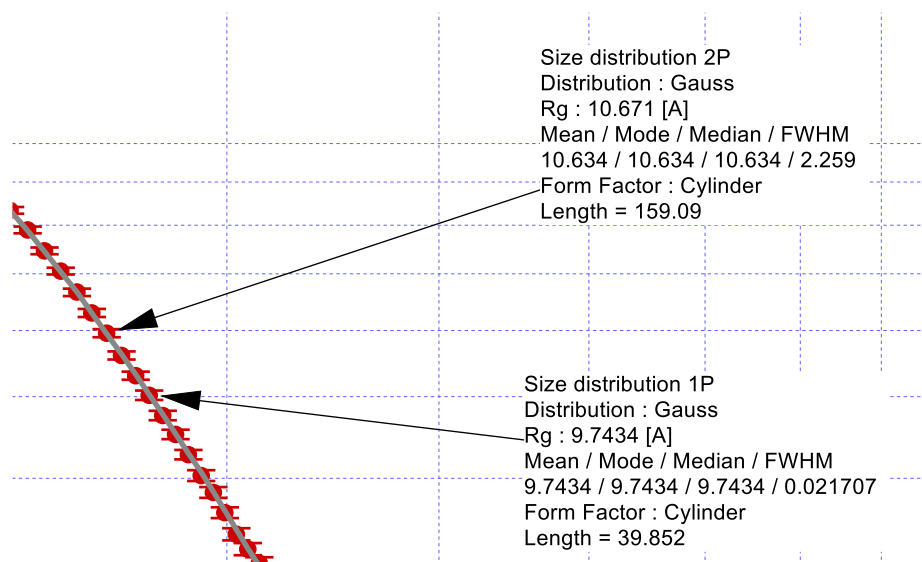
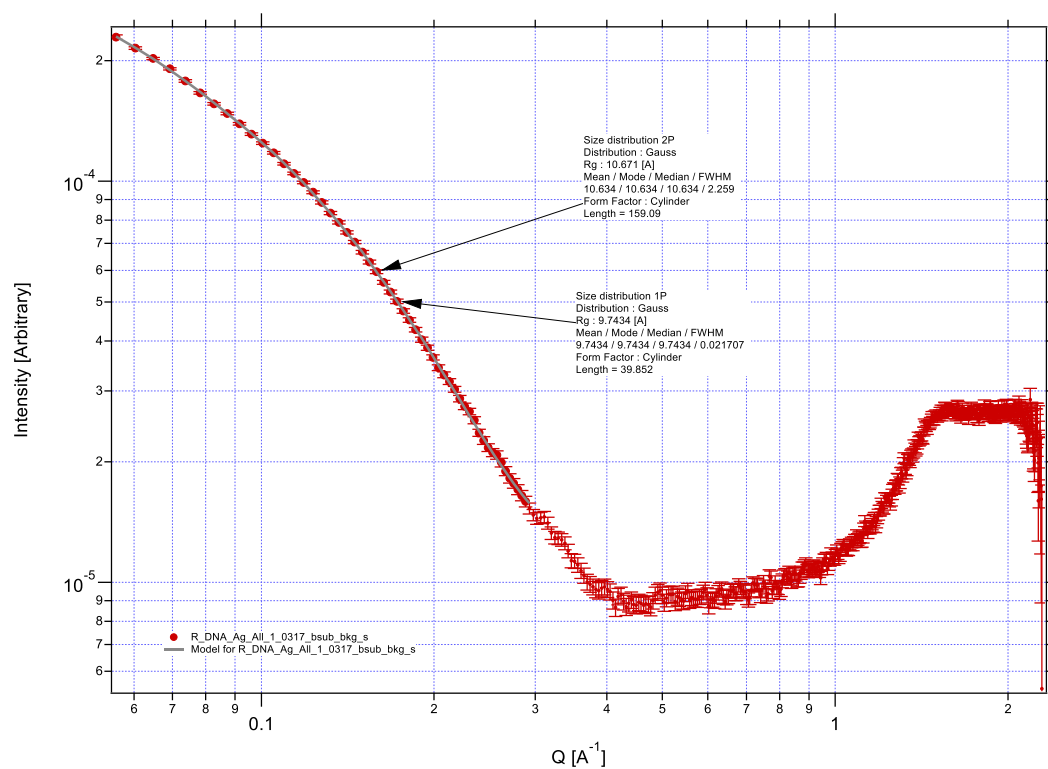
1.9 SAXS fitting figures for duplex II (0.2 mM) (away K-edge; 24.514 keV)
(Advanced Photon Source)



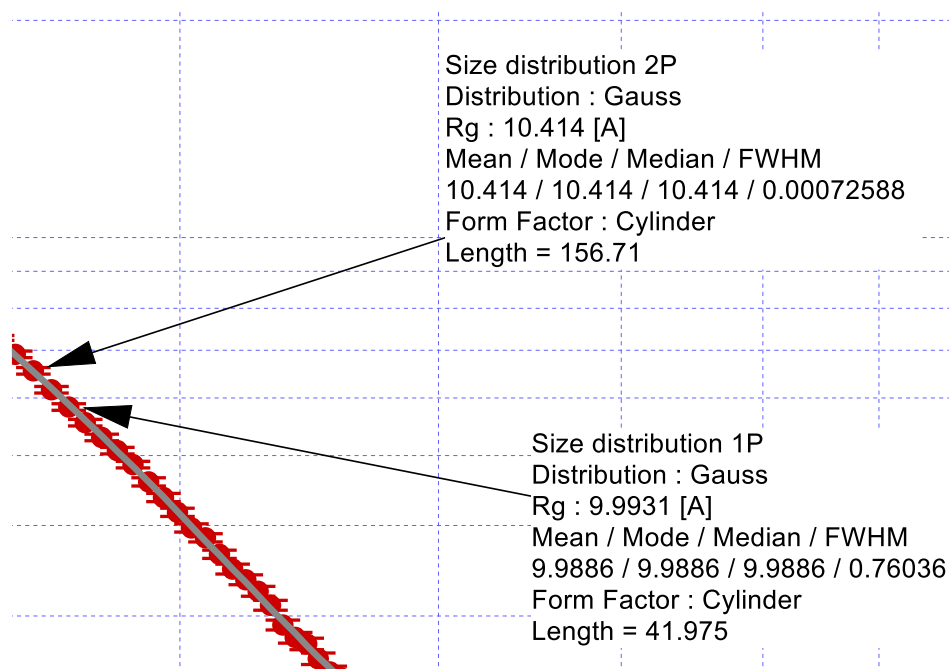
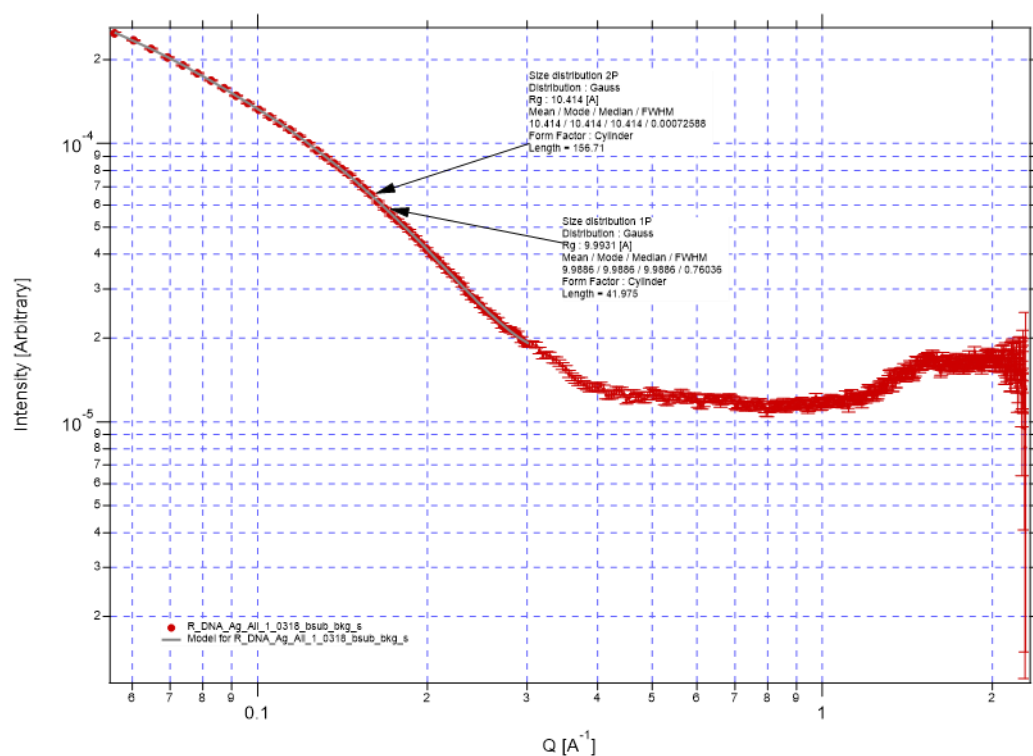
Supplementary Figure 20 | Cylindrical model of canonical duplex II (0.2 mM) in absence of Ag^I (away from K-edge; 24.514 keV).



Supplementary Figure 21 | Cylindrical model of canonical duplex II (0.2 mM) upon adding 1 equivalent of Ag^+ per base pair (away from K-edge; 24.514 keV).



Supplementary Figure 22 | Cylindrical model of canonical duplex II (0.2 mM) upon adding 1.5 equivalents of Ag^I per base pair (away from K-edge; 24.514 keV).



Supplementary Figure 23 | Cylindrical model of canonical duplex II (0.2 mM) upon adding 2 equivalents of Ag^I per base pair (away from K-edge; 24.514 keV).

Supplementary Table 2 | Cylindrical fitting parameters for anomalous X-ray scattering of Duplex I in the presence of Ag^I ions.

Fitting parameters		
¹ Duplex I (0.2 mM)		
Equivalents Ag ^I /base pair	Radius (Å)	Length (Å)
0	11.8	40.18
1.0	10.55	38.74
1.5	10.23	39.95
2	10.34	41.05
¹ from APS synchrotron SAXS (silver K-edge; 24.514 keV).		

Supplementary Table 3 | Duplex I core-shell cylinder fit comparing Ag-core density at the silver K-edge (25.514 keV)³ and below the silver K-edge (24.514 keV)

Sample (X-ray energy)	Cylinder diameter (total, Å)	Cylinder core thickness ² (Å)	Cylinder shell thickness (Å)	Core density ¹	Shell density ¹	Cylinder length (Å)
1 eq. Ag ^I /bp (25.514 keV)	18.06	9.7	4.2	108	19.5	36.5
1 eq. Ag ^I /bp (24.514 keV)	18.06	9.7	4.2	117	19.5	36.5
1.5 eq. Ag ^I /bp (25.514 keV)	18.14	10.0	4.7	110	21.4	37.1
1.5 eq. Ag ^I /bp (24.514 keV)	18.14	10.0	4.7	120	21.4	37.1
2 eq. Ag ^I /bp (25.514 keV)	19.8	11.0	4.4	113	19.6	40.0
2 eq. Ag ^I /bp (24.514 keV)	19.8	11.0	4.4	122	19.6	40.0

¹ X-ray scattering length density (10^{10} cm^{-1}), normalized to solvent (water) scattering defined with a fixed value of 10.

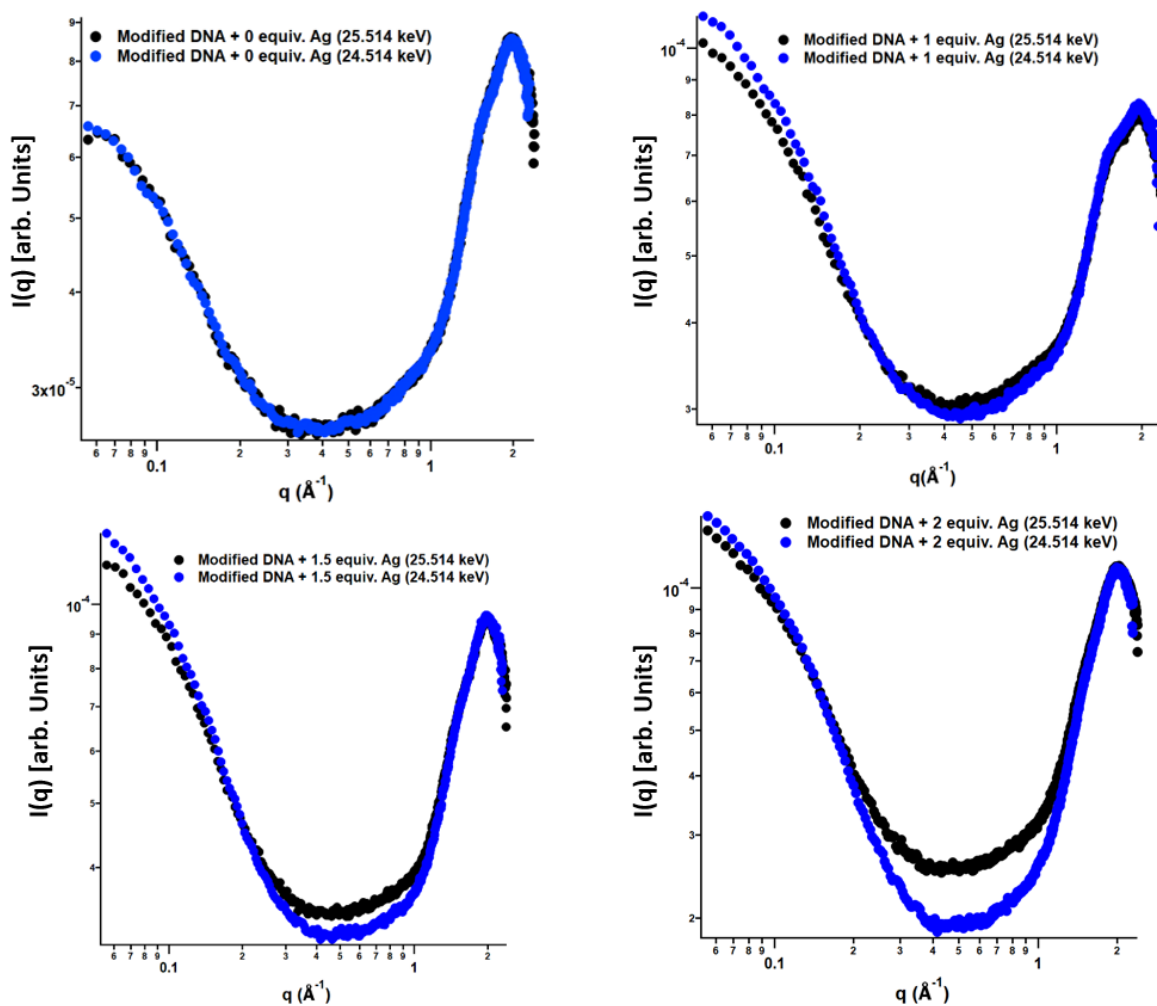
² Core thickness + 2·(shell thickness)

³ All parameters are freely refined for data collected below the silver K-edge (24.514 keV), and only the core density is freely refined for data collected at the silver K-edge (25.514 keV).

Supplementary Table 4 | Duplex II core-shell cylinder fit comparing Ag-core density at the silver K-edge (25.514 keV) and below the silver K-edge (24.514 keV)

Sample (X-ray energy)	Cylinder diameter (total, Å)	Cylinder length (Å)	% phase 1	Cylinder diameter (total, Å)	Cylinder length (Å)	% phase 2
Phases fitted	Phase 1			Phase 2		
0 eq. Ag/bp (25.514 keV)	19.90	37.25	100	N/A		
0 eq Ag/bp, (24.514 keV)	22.98	39.29	100	N/A		
1 eq. Ag/bp (25.514 keV)	20.00	44.38	100	N/A		
1 eq Ag/bp, (24.514 keV)	20.96	43.22	100	N/A		
1.5 eq Ag/bp (25.514 keV)	20.14	58.44	100	N/A ¹		
1.5 eq Ag/bp, (24.514 keV)	19.48	39.85	33	21.26	159.09	67
2 eq Ag/bp (25.514 keV)	21.20	70.80	100	N/A ¹		
2 eq Ag/bp (24.514 keV)	19.98	41.98	15	20.82	156.71	85

¹ Could not be fitted with two phases that reasonably represented isolated DNA helices plus linked DNA helices



Supplementary Figure 24 | Comparison of scattering of duplex I in the presence and absence of Ag^I at two different scattering energies, below the Ag K-edge (24.514 keV, blue curves) and at the Ag K-edge (25.514 keV, black curves).

1.10 ASAXS Analysis

The energy-dependent electron density contrast from a system with energies very close to the X-ray absorption of an element (termed as the resonant element) within the system can be written as:^{1,2,3,4,5,6}

$$\rho_e(\vec{r}, E) = \rho_{eo}(\vec{r}) - \rho_{es} + v(\vec{r})(f'(E) + if''(E)) \quad (\text{Supplementary equation 1})$$

Where $\rho_{eo}(\vec{r})$ is the energy-independent total electron density of the sample and ρ_s is the electron density of solvent (in our case the solvent is water with $\rho_{es} = 0.334 \text{ e}/\text{\AA}^3$), whereas $v(\vec{r})$ is the number density of the resonant element only in the system.

Taking the fourier transform one can obtain the X-ray scattering as:^{1,2,3,4,5,6}

$$\begin{aligned} I(\vec{q}, E) &= \frac{N}{V} r_e^2 \left| \int \rho_e(\vec{r}, E) e^{i\vec{q} \cdot \vec{r}} d\vec{r} \right|^2 \\ &= |\rho_{os}(\vec{q})|^2 + f'(E) \text{Re}[\rho_{os}(\vec{q}) \rho_r^*(\vec{q}) + \rho_{os}^*(\vec{q}) \rho_r(\vec{q})] \\ &\quad + (f'^2(E) + f''^2(E)) |\rho_r(\vec{q})|^2 \end{aligned} \quad (\text{Supplementary equation 2})$$

Where, N/V is the number of scattering samples per unit volume, r_e is the classical electron radius, $\rho_{os}(\vec{q}) = \int (\rho_{eo}(\vec{r}) - \rho_{es}) e^{i\vec{q} \cdot \vec{r}} d\vec{r}$ and $\rho_r(\vec{q}) = \int v(\vec{r}) e^{i\vec{q} \cdot \vec{r}} d\vec{r}$ are complex numbers, Re denotes real part of the complex number. But for systems centrosymmetric geometries like sphere, cylinder, ellipsoid, etc, these terms becomes real and isotropic in \vec{q} . Owing to that, the above Supplementary equation can be further simplified into

$$\begin{aligned} I(q, E) &= \rho_{os}^2(q) + 2f'(E) \rho_{os}(q) \rho_r(q) \\ &\quad + (f'^2(E) + f''^2(E)) \rho_r^2(q) \end{aligned} \quad (\text{Supplementary equation 3})$$

The first term in this Supplementary equation 3 is energy independent and can be termed as *SAXS-term* ($I_s = \rho_{os}^2(q)$). Whereas both the 2nd and 3rd terms have energy dependence. The 2nd term contains the *Cross-term* ($I_c = \rho_{os}(q) \rho_r(q)$) and has the contribution from the resonant element as well as all other atoms in the system. Whereas the 3rd term has the *Resonant-term* ($I_r = \rho_r^2(q)$) that only has contribution

from the resonant element. In general, just below the absorption edge of the resonant there is the imaginary part of the scattering constants ($f'(E), f''(E)$) of the resonant element does not change considerably. Hence, the above Supplementary equation is basically a quadratic function of the real part of the scattering constant of the resonant element ($f'(E)$).

As per ASAXS experiments we obtained the scattering intensity as a function of q and E , i.e. the left-hand side of eq. 3. In general, the complex scattering constants of the resonant element can be obtained from well tabulated values from National Institute of Standards and Technology online database.⁷ With the tabulated values for resonant element one can have system of linear equations based on Supplementary equation 3 after solving which one can obtain the values of I_S , I_C , and I_R .

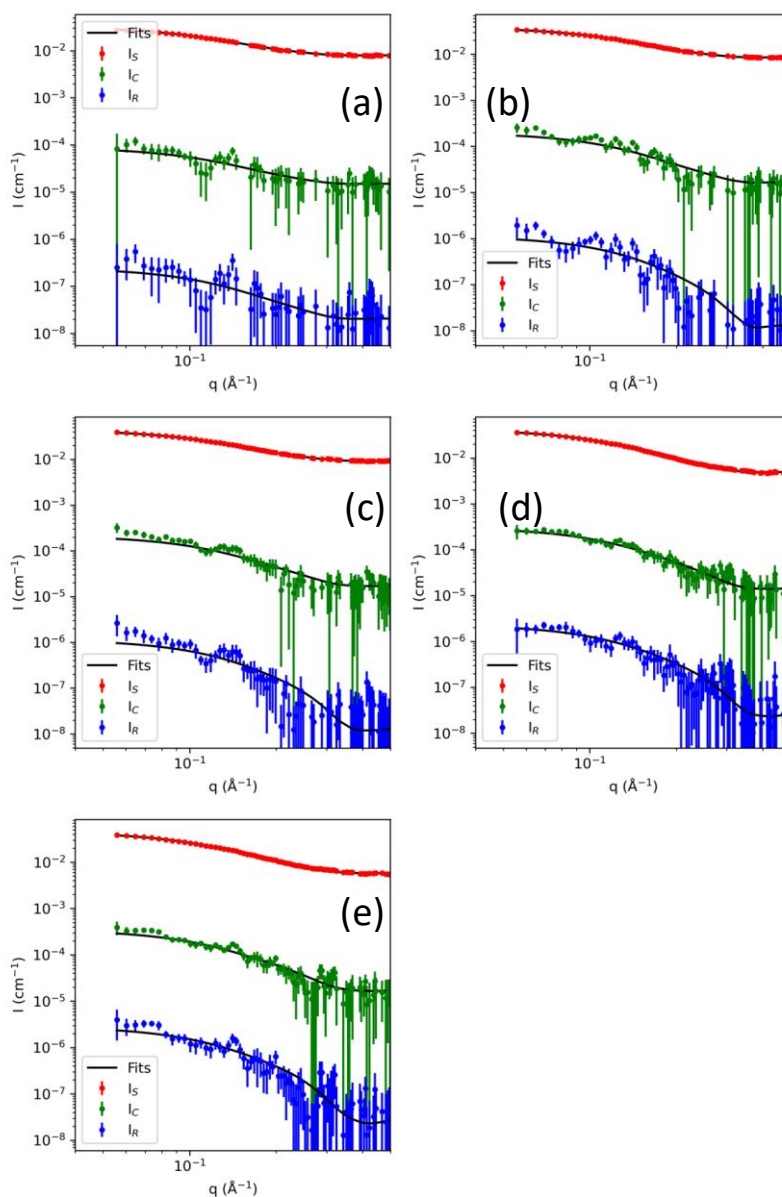
The *Resonant-term* in the Supplementary equation, in general, is few orders of magnitude smaller than the other terms and for most of the practical purposes the Supplementary equation can be further approximated into:

$$I(q, E) \approx \rho_{os}^2(q) + 2f'(E)\rho_{os}(q)\rho_r(q) \quad (\text{Supplementary equation 4})$$

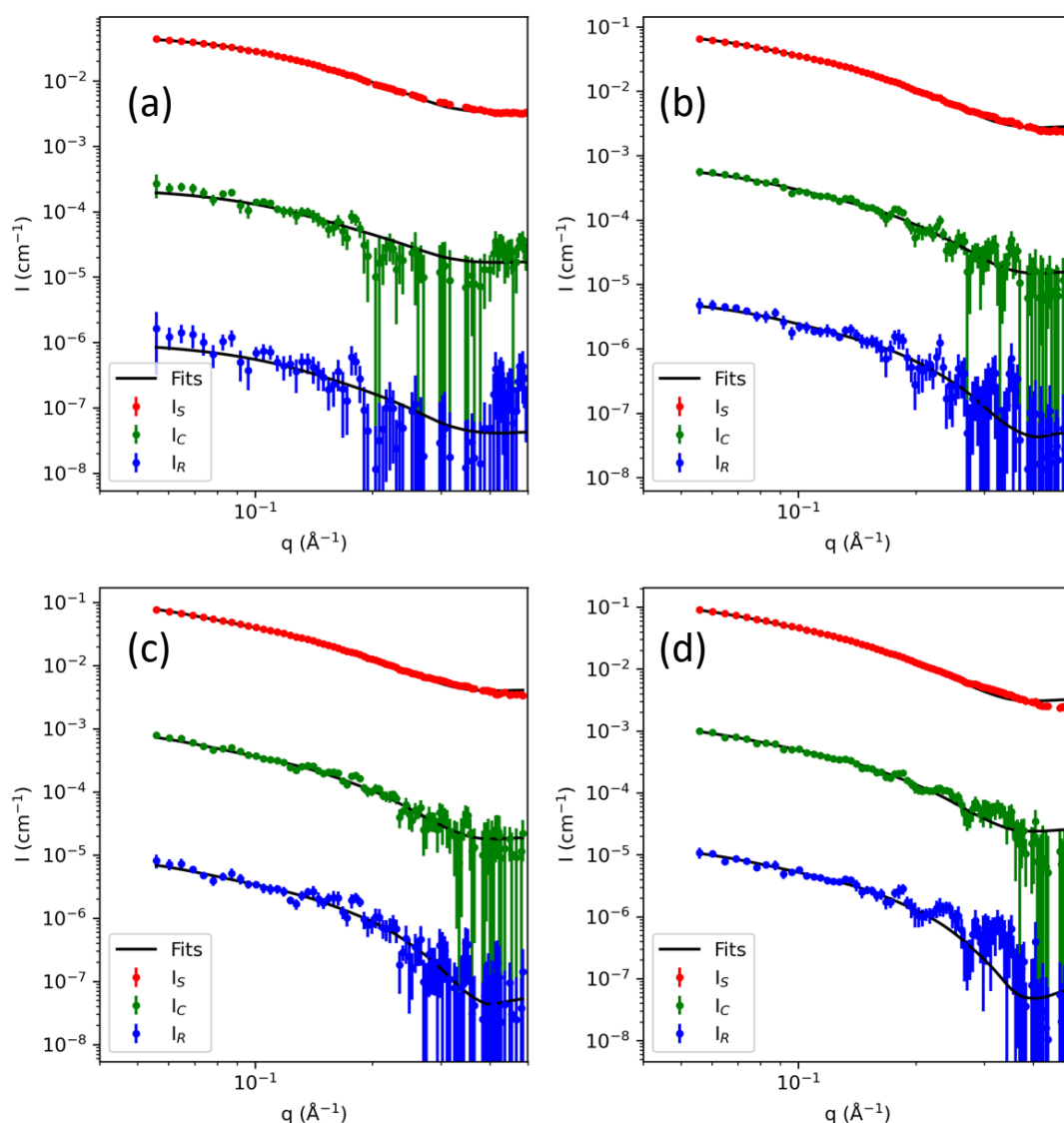
Hence, firstly the *Resonant-term* can be extracted from the *Cross-term* as:

$$I_R(q) = \rho_r^2(q) = I_C^2(q)/I_S(q) \quad (\text{Supplementary equation 5})$$

We applied this constraint to solve the linear Supplementary equations obtained from experimental data using Supplementary equation 3 to obtain I_S , I_C , and I_R as shown in Supplementary Figure 25 and 26 for duplex I and duplex II, respectively. The splitting of the data is done using the python package XAnoS_Components.py under XAnoS software developed at NSF's ChemMatCARS.⁸



Supplementary Figure 25 | The scattering components - SAXS-term (I_S), Cross-term (I_C), and Resonant-term (I_R) obtained from energy dependent SAXS data below the X-ray absorption K-edge of Ag from duplex I with different AgI equivalents of (a) 0.5, (b) 1.0, (c) 1.5, (d) 2.0, and (e) 3.0 . The solid black lines are fits to the solid cylinder model of the Ag-DNA complexes.



Supplementary Figure 26 | The scattering components - SAXS-term (I_S), Cross-term (I_C), and Resonant-term (I_R) obtained from energy dependent SAXS data below the X-ray absorption K-edge of Ag from duplex **II** with different Ag^I equivalents of (a) 1.0, (b) 1.5, (c) 2.0, and (d) 3.0. The solid black lines are fits to the solid cylinder model of the Ag-DNA complexes.

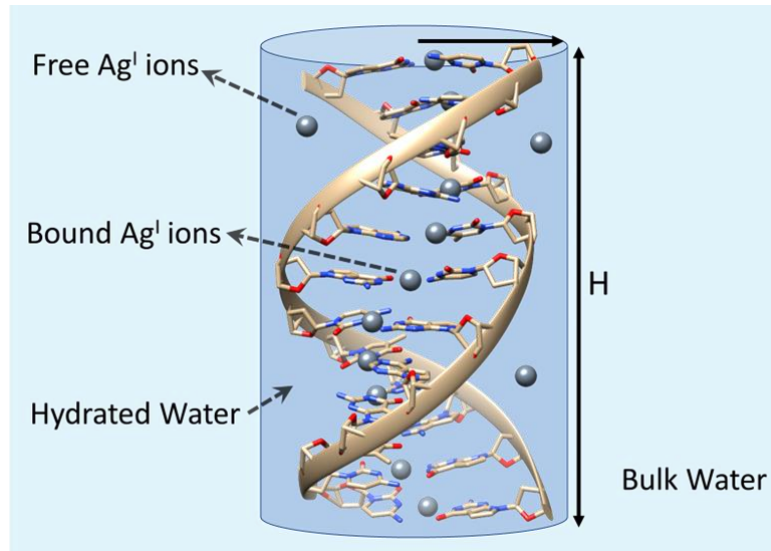
And secondly, the change in scattering intensity as a function of energy can be written as:

$$I(q, E_1) - I(q, E_2) \approx 2(f'(E_1) - f'(E_2))I_C \quad (\text{Supplementary equation 6})$$

Or one can simply write:

$$\Delta I \propto \Delta f' \quad (\text{Supplementary equation 7})$$

Solid Cylinder Model of DNA-Ag complex: In order to obtain the number of Ag-atoms within the double-stranded DNA structure, we model both the DNA-Ag complexes (duplex I and duplex II) as randomly dispersed and oriented monodisperse solid cylinders of radius, R , and height, H , in water as shown in Supplementary Figure 27.



Supplementary Figure 27 | Solid cylinder structure to model the Ag-DNA complexes in water.

The solid cylindrical region is comprised of the DNA-Ag complex and the hydrated water molecules within it. Hence, the electron density within the cylindrical region will have contributions from the elements from DNA-Ag complexes, free-Ag ions and water molecules. We write the chemical composition of each of the base pair as $C_{20}H_{23}N_7O_{12}P_2Ag_x \cdot (H_2O)_{N_w}$, where x is the number of moles of Ag per base-pair (including Free-Ag ions and DNA-Complexed-Ag atoms) and will be determined by fitting the experimental data and N_w is the number of moles of water molecules hydrating the base-pair within the solid cylinder region. The mass density of the base-pair ($C_{20}H_{23}N_7O_{12}P_2$) part only without Ag is calculated to be $\rho_{BP} = 0.96 \text{ gm/cm}^3$ considering 12 base-pairs within a cylinder of radius, $R = 10 \text{ \AA}$, and height $H = 40 \text{ \AA}$.

Depending upon the values of x -moles of Ag per base-pairs, the mass density of the base-pair including Ag atoms and ions, $\rho_{BP Ag}$, is rescaled as per the atomic weight of the x -moles of the Ag:

$$\rho_{BP Ag} = \rho_{BP} * (M_{W_{BP}} + x \cdot W_{Ag}) / M_{W_{BP}} \quad (\text{Supplementary equation 8})$$

Where $(M_{W_{BP}}, \rho_{BP})$ are Molecular weight and mass density of base pairs without silver, and $M_{W_{BP Ag}} = (M_{W_{BP}} + x \cdot W_{Ag})$ is the molecular weight of base pairs including Ag with atomic weight, W_{Ag} . As per our data modeling with the cylindrical modeling, the crucial information is to figure out the density of the hydrating water molecules within the cylindrical regions which will determine the value of N_w . The value of N_w is determined from the rescaled density of hydrated water molecules (ρ_{sHW}) which can be written as:

$$N_w = \frac{\rho_{sHW}}{M_{W_{H_2O}}} = \frac{\rho_{HW}}{M_{W_{H_2O}}} \left(1 - \frac{\rho_{BP Ag} \cdot V_{M_{BP Ag}}}{M_{W_{BP Ag}}} \right) \quad (\text{Supplementary equation 9})$$

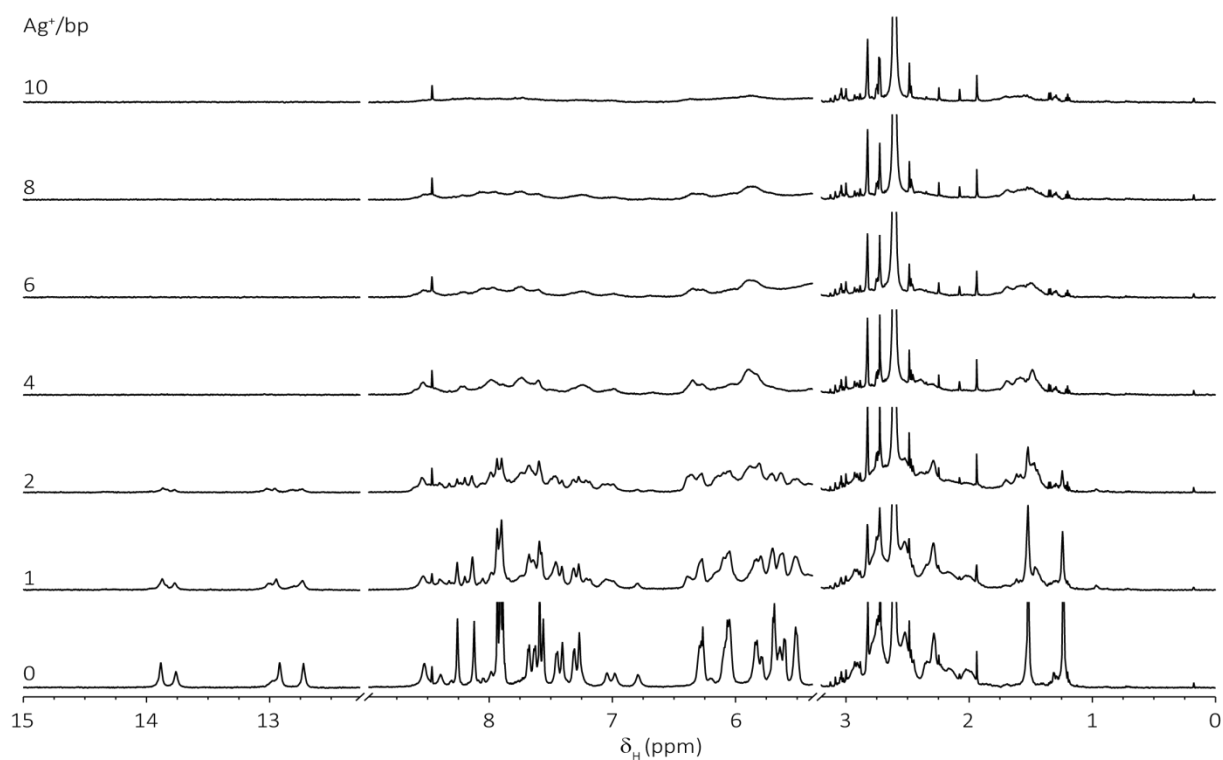
Where ρ_{HW} is the density of hydrated water, $M_{W_{H_2O}}$ is molecular weight of water, and $(M_{W_{BP Ag}}, V_{M_{BP Ag}}, V_{M_{H_2O}})$ are molecular weights, molar volume the Ag containing base-pair ($C_{20}H_{23}N_7O_{12}P_2Ag_x$), and molar volume of H_2O , respectively. The rescaling of the solvated water is needed to take care of the volume replaced by the Ag containing base-pair. The molar volume is approximated by considering the shapes of all atoms as spheres with Van der Waal's radii (obtained from python Mandeleev package⁹). Hence, the overall mass density of the cylindrical region, combining the contribution of base-pairs, Ag, and the hydrated water molecule, can be written as

$$\rho_o = \rho_{BP Ag} + \rho_{HW} \left(1 - \frac{\rho_{BP Ag} \cdot V_{M_{BP Ag}}}{M_{W_{BP Ag}}} \right) \quad (\text{Supplementary equation 10})$$

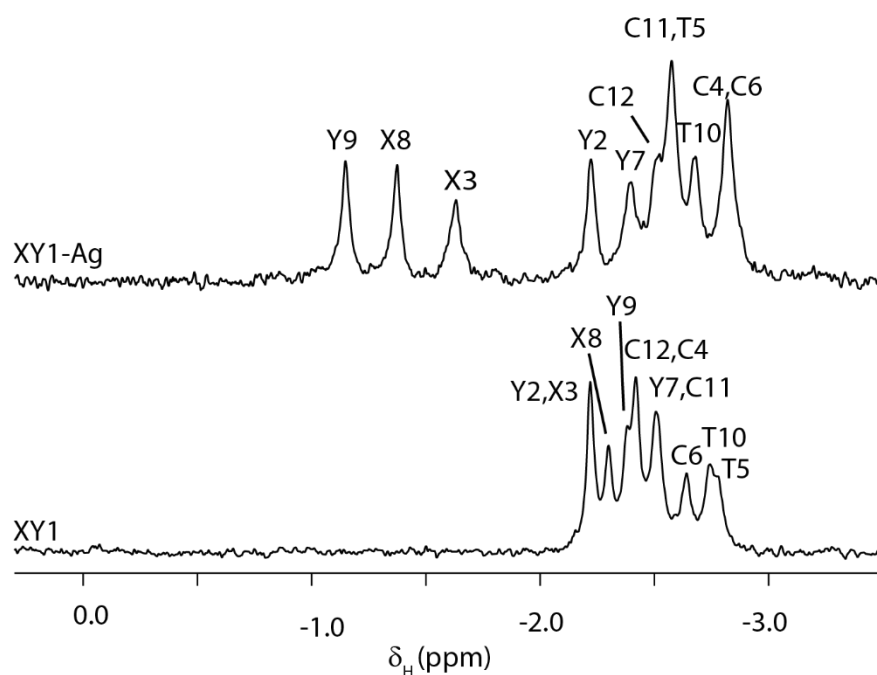
We consider the hydrated water density within the cylindrical region to be the same as bulk water and take the density as $\rho_{HW}(= \rho_s) = 1 \text{ gm/cm}^3$.

With the above mentioned approach, we calculated the energy-dependent electron density of the cylindrical region from the contribution of each of the elements in the system by taking the contribution of each of the elements in the system. Atomic numbers of elements are used to provide the contribution except the resonant element, Ag, for which energy dependent complex atomic scattering constant is provided from the database from NIST webpage as mentioned above.

1.11 NMR spectroscopy



Supplementary Figure 28 | ^1H NMR spectra of titration of the canonical analogue duplex II (5'-d(GGA CTC GAG TCC)-3' with Ag^{I} ions. Spectra were recorded at 5 °C, 0.2 mM DNA (ds-DNA) concentration and Ag^{I} ions were added up to a final concentration of 40 mM.



Supplementary Figure 29 | ^{31}P NMR spectra of the duplex **I** before and after adding 2 equivalents of Ag^{I} ions per base pair with assignments.

1.12 Comparison of average structural parameters for **I** and **I-Ag** structures

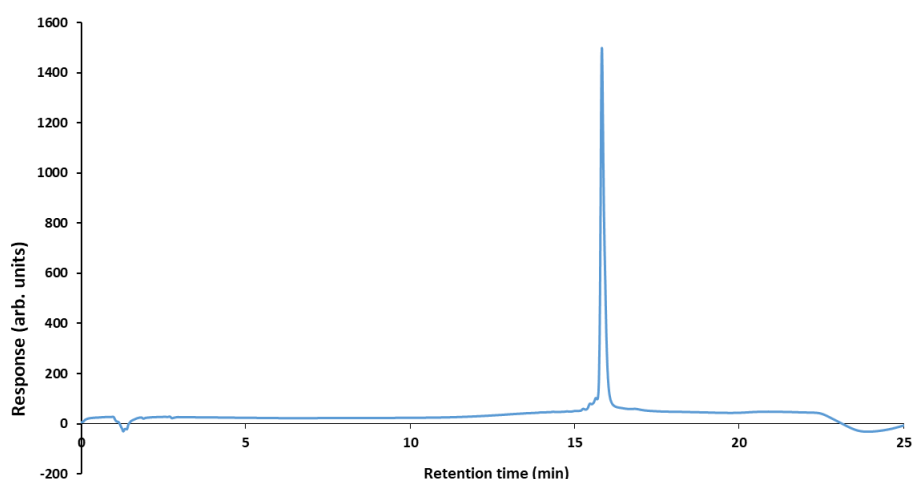
Supplementary Table 5. Comparison of average structural parameters for **I**, **I-Ag** (NMR) and **I-Ag** (DFT) structures along with typical B-DNA values.

parameter	I	I-Ag (NMR)	I-Ag (DFT)	B-DNA
buckle [°]	1 ± 5	0 ± 10	2 ± 9	0.2
propeller [°]	-8 ± 3	-21 ± 4	-8 ± 9	-11
opening [°]	0 ± 1	-35 ± 1	-28 ± 10	0
slide [Å]	-0.8 ± 0.4	-1.4 ± 0.3	-1 ± 1	0.4
rise [Å]	3.3 ± 0.1	3.3 ± 0.1	3.3 ± 0.3	3.4
tilt [°]	0 ± 2	0 ± 1	0 ± 3	0
roll [°]	5 ± 3	2 ± 4	4 ± 4	1
twist [°]	33 ± 1	34 ± 4	34 ± 6	36
minor groove [Å]	13 ± 0	15 ± 1	15 ± 1	11.5
major groove [Å]	19 ± 1	18 ± 1	17 ± 1	17.5
radius (P)	10.5 ± 0.7	10.7 ± 0.3	10 ± 2	9.4

Supplementary Table 6. Neighbouring Ag^I ion distances in **I-Ag** (NMR) and **I-Ag** (DFT) structures.

step	I-Ag (NMR)	I-Ag (DFT)
1	3.83 ± 0.05	4.69
2	3.79 ± 0.07	3.15
3	3.27 ± 0.03	3.25
4	3.70 ± 0.04	3.56
5	4.01 ± 0.06	3.48
6	4.39 ± 0.09	3.41
7	4.02 ± 0.04	3.57
8	3.71 ± 0.04	3.97
9	3.28 ± 0.02	3.33
10	3.77 ± 0.07	4.44
11	3.84 ± 0.04	3.25
average	3.8 ± 0.3	3.6 ± 0.5

1.13 RP-HPLC oligonucleotide analysis for ODN1



Time (min)	Buffer A*	Buffer B**	Flow [mL/min]
0	100	0	0.8
20	70	30	0.8
21	100	0	0.8
25	100	0	0.8

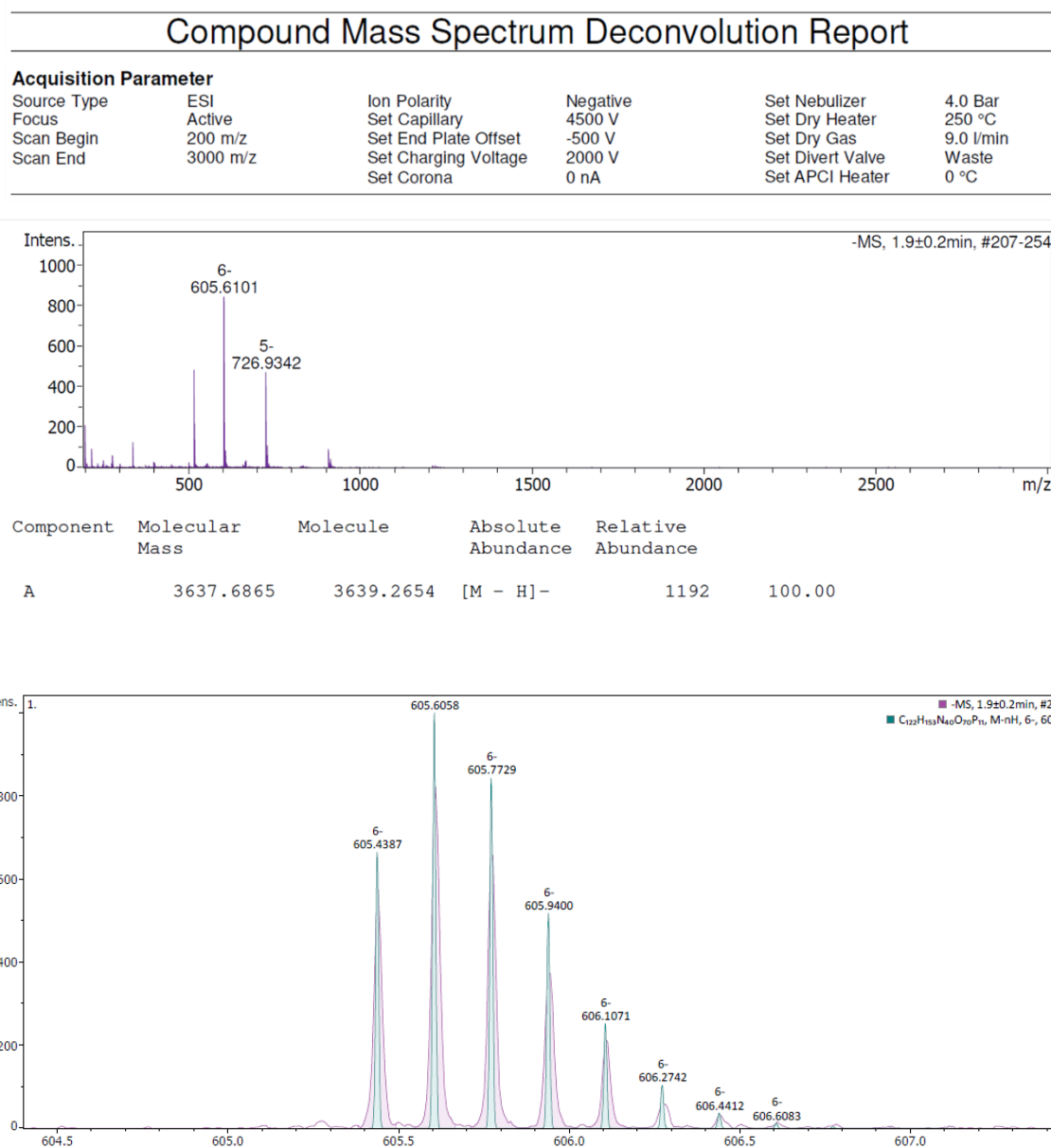
*Buffer A: 0.1M Triethylammonium acetate pH 6.5 + 5% CH₃CN

**Buffer B: 0.1M Triethylammonium acetate pH 6.5 + 65% CH₃CN

Supplementary Figure 30. RP-HPLC chromatogram (C18 column) of purified oligonucleotide ODN1, accompanied by a table detailing the elution method utilized.

Note: The oligonucleotide ODN2 was purchased from Sigma-Aldrich with HPLC purification grade.

1.14 Mass Spectrometry for oligonucleotide ODN1 and ODN2

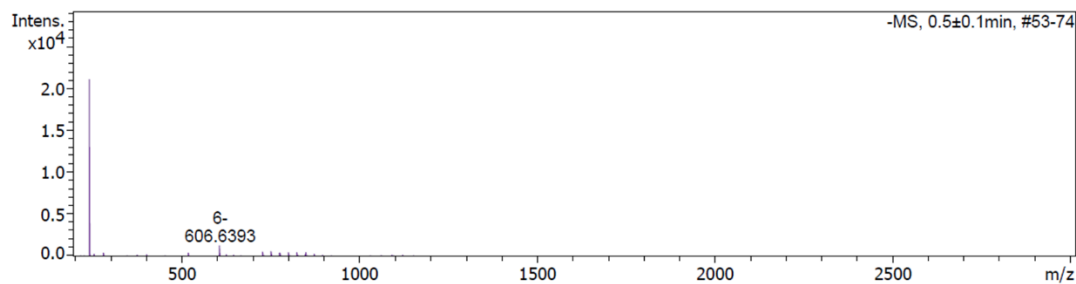


Supplementary Figure 31. ESI-MS (negative mode) spectra for oligonucleotide ODN1. The top image presents the deconvolution report for the spectrum with a charge state of $z = -6$. The bottom image provides a comparison between the theoretical spectrum (blue) and the experimental spectrum (purple).

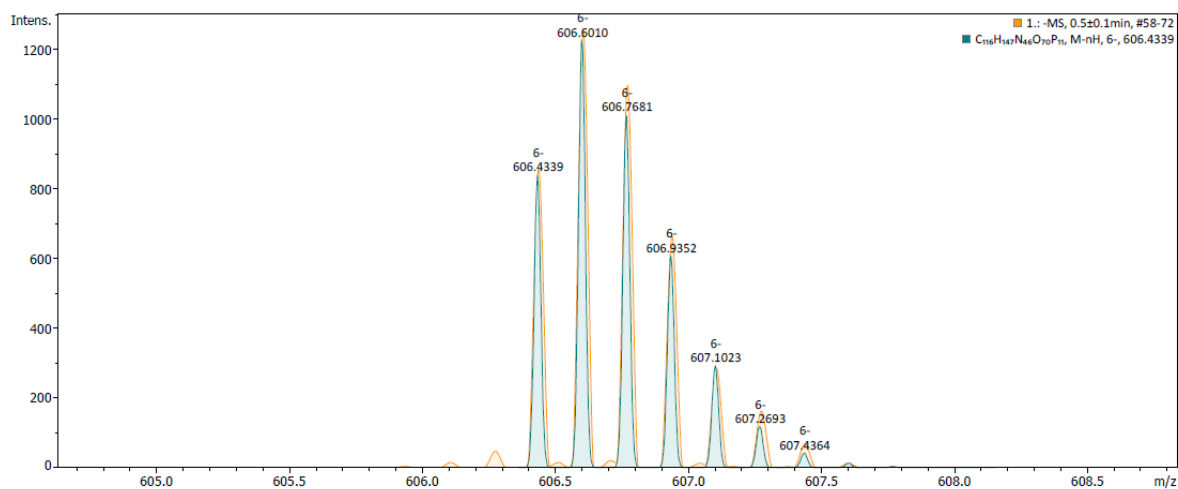
Compound Mass Spectrum Deconvolution Report

Acquisition Parameter

Source Type	ESI	Ion Polarity	Negative	Set Nebulizer	4.0 Bar
Focus	Active	Set Capillary	4500 V	Set Dry Heater	250 °C
Scan Begin	200 m/z	Set End Plate Offset	-500 V	Set Dry Gas	9.0 l/min
Scan End	3000 m/z	Set Charging Voltage	2000 V	Set Divert Valve	Waste
		Set Corona	0 nA	Set APCI Heater	0 °C



Component	Molecular Mass	Molecule	Absolute Abundance	Relative Abundance
A	3643.8686	3645.5057 [M - H] ⁻	1530	100.00



Supplementary Figure 32. ESI-MS (negative mode) spectra for canonical oligonucleotide ODN2. The top image presents the deconvolution report for the spectrum with a charge state of $z = -6$. The bottom image provides a comparison between the theoretical spectrum (green) and the experimental spectrum (orange).

2. SUPPLEMENTARY REFERENCES

-
- ¹ Stuhmann, H. B. Anomalous Dispersion of Small-Angle Scattering of Horse-Spleen Ferritin at the Iron K-Absorption Edge. *Acta Crystallogr. A* **36**, 996-1001 (1980). <https://doi.org:10.1107/S0567739480002033>
- ² Ballauff, M. & Jusufi, A. Anomalous small-angle X-ray scattering: analyzing correlations and fluctuations in polyelectrolytes. *Colloid Polym. Sci.* **284**, 1303-1311 (2006). <https://doi.org:10.1007/s00396-006-1516-5>
- ³ Tatchev, D. Structure analysis of multiphase systems by anomalous small-angle X-ray scattering. *Philos. Mag.* **88**, 1751-1772 (2008). <https://doi.org:10.1080/14786430802279760>
- ⁴ Sztucki, M., Di Cola, E. & Narayanan, T. New opportunities for Anomalous Small-Angle X-Ray Scattering to characterize Charged Soft Matter Systems. *J. Phys. Conf. Ser.* **272** (2011). <https://doi.org:10.1088/1742-6596/272/1/012004>
- ⁵ Sztucki, M., Di Cola, E. & Narayanan, T. Anomalous small-angle X-ray scattering from charged soft matter. *Eur. Phys. J-Spec. Top* **208**, 319-331 (2012). <https://doi.org:10.1140/epist/e2012-01627-x>
- ⁶ Wieland, D. C. F. *et al.* ASAXS measurements on ferritin and apoferritin at the bioSAXS beamline P12 (PETRA III, DESY). *J. Appl. Crystallogr.* **54**, 830-838 (2021). <https://doi.org:10.1107/S1600576721003034>
- ⁷ Chantler, C. T. *J. Phys. Chem. Ref. Data* **29**, 597-1048 (2000).
- ⁸ Bera, M. K. *X-ray Anomalous Scattering (XAnoS)* (2022). <https://github.com/nayanbera/XAnoS.git>
- ⁹ Mentel, L. *A Python resource for properties of chemical elements, ions and isotopes* (2014). <https://github.com/lmmentel/mendeleev>